Deep structure of the Pará-Maranhão/Barreirinhas passive margin in the Equatorial Atlantic (NE Brazil)

Maryline Moulin, Daniel Aslanian, Flora Gallais, Alexandra Afilhado, Philippe Schnurle, Mikael Evain, José Soares, Reindhart Fuck, Otaviano da Cruz Pessoa Neto, Adriano Viana, et al.

Version of Record: https://www.sciencedirect.com/science/article/pii/S0895981121001693
Manuscript_95385bf7c67daf4bc747c9069fae8f79

Deep structure of the Pará-Maranhão/Barreirinhas passive margin in the Equatorial Atlantic (NE Brazil)

Daniel Aslanian[1], Flora Gallais[1], Alexandra Afilhado[2,3], Philippe Schnurle[1], Maryline Moulin[1], Mikael Evain[1], Nuno Dias[2,3], Jose Soares[4], Reinhart Fuck[4], Otaviano da Cruz Pessoa Neto [5], Adriano Viana[5] and the MAGIC Team[6]

(1) Ifremer, Department of Marine Geosciences, BP 70, Plouzané, France

(2) ISEL - Instituto Superior de Engenharia de Lisboa, Lisboa, Portugal

(3) IDL – Instituto Dom Luis, Lisboa, Faculdade das Ciências da Universidade de Lisboa, 1749-016 Lisboa, Portugal.

(4) Instituto de Geociencias, Universidade de Brasília, Campus Darcy Ribeiro, 70910-900 Brasilia, Brazil

(5) Petrobras, Cenpes Research Center, Rio de Janeiro, Brazil

(6) Morvan, L., Mazé, J.P., Pierre, D., Roudaut-Pite, M., Rio, Alves, D., Barros Junior, P., Biari, Y., Corela, C., Crozon2, , Duarte, J.L., Ducatel, C., Falcão, C., Fernagu, P., Vinicius Aparecido Gomes de Lima, M., Le Piver, D., Mokeddem, Z., Pelleau, P., Rigoti, C., Roest, W. & Roudaut, M.

Abstract

The Pará-Maranhão/Barreirinhas margin, North Brazil, is a pull-apart passive margin, with two strike-slip borders, formed during the opening of the Equatorial Atlantic Ocean during Cretaceous time. Its geometry and evolution are speculative due to the lack of information on the crustal structure and the crustal nature. We present here the E-W profiles of the MAGIC (**M**argins of br**A**zil, **G**hana and **I**vory **C**oast) deep seismic experiment, a joint project between French and Brazilian universities, research institutes and the industry. Fifty-six Ocean Bottom Seismometers (OBS) and a 4.5 seismic streamer were deployed at sea along 2 of the 5 MAGIC profiles. One profile was extended onshore by installing 8 land stations. We perform forward modelling through combined interpretation of the multichannel seismic and of the main reflected and refracted of these phases recorded by the OBSs. The final P-wave velocity models reveal distinct structural domains from onshore Brazil towards the Atlantic Ocean characterized by variations of the crustal thicknesses and velocities: (1) an unthinned continental crust below the São Luís Craton, where the crust is 33 km thick, (2) a 60 km wide necking domain below the Ilha de Santana Platform; (3) offshore, east of the continental slope, a 10km-thick deep sedimentary basin underlain by a 5km thick crust with velocity of 6.2-6.9 km/s that we interpret as an exhumed lower continental crust, on the top of an Anomalous Velocity Layer (AVL) probably made of intrusions of mantle-derived melts into the lower continental crust, or a mixture of them; (4) eastwards, the limit of the previous domain is marked by NW-SE aligned volcanoes and the disappearance of the AVL. The sedimentary succession becomes thinner (6 km) overlaying a proto-oceanic crust characterized by seismic velocities higher than “normal” oceanic crust in its upper part, but in continuity with the velocity described in the previous domain; (5) followed by a more

characteristic but thin oceanic crust.

The middle/lower continental crust seems not only to have a crucial role in the genesis of the passive margin but also to be involved in the genesis of the first oceanic crust. The passage to a typical oceanic crust seems to have occurred progressively by steps: first in the deeper layer by the setup of more and more intrusions of mantle-derived melts at the base of the crust or mixture of exhumed lower crust and mantle, producing a domain of proto-oceanic crust, then by the emplacement of an upper 1-2km-thick layer with typical oceanic characteristics.

Keyword: Equatorial Atlantic Ocean, Pará-Maranhão/Barreirinhas margin, Northeast Brazil, passive margin, crustal structure, lower continental crust, proto-oceanic, wide-angle seismic

1 *Introduction*

The opening of the Central Atlantic Ocean started in Sinemurian time (~195 My ; Sahabi et al., 2004), whereas the South Atlantic Ocean in Hauterivian time (~135 My ; Moulin et al., 2010), about 60 My later. The opening of the South Atlantic Ocean was shifted of about 30° to the east with respect to the Central Atlantic Ocean. In that context, the Equatorial Atlantic Ocean represents a « transfer area » between these two break-ups (Moulin et al., 2010).

The Equatorial Atlantic ocean is separated from the Central Atlantic Ocean, to the north, by the Guinea Fracture Zone and from the South Atlantic Ocean, to the south, by the Chain Fracture Zone. The break-up in the Equatorial Atlantic Ocean occurred through a Precambrian Craton and created two very unequal pieces (Figure 1A, Moulin et al., 2010): the West African Craton, fringed to the SW and the SE by the Rokelides and Dahomeyides Panafrican belts, respectively (Villeneuve, 2005; Villeneuve et al., 2010; Deynoux et al., 2006) and the São Luís Craton (Klein et al., 2005).

This 2000 km long Equatorial Atlantic Ocean can still be divided into three 600-800 km long main sub-segments, separated by main fracture zones (Figure IA). Segment I is limited by the Sierra Leone Fracture Zone to the north and the São Paulo Fracture Zone to the south. It is divided into two ~ 400 km-large segments separated by the 4°N Fracture Zone and fringed by a) the Demerara plateau-Sierra Leone conjugate passive margins system and b) the Foz do Amazonas-Liberian conjugate passive margins system. This segment 1 is formed by mainly divergent passive margins, that are separated by short strike-slip/highly oblique zones. Segment III is limited by the Chain Fracture Zone to the North and the Ascension Fracture Zone to the south. It represents a 600 km divergent large segment, bordered by the Pernambuco-Parnaíba and Cameroon system. In-between, Segment II is bounded by the São Paulo Fracture Zone to the north and the Chain Fracture Zone. It is divided into two smaller segments, about 300 km wide, separated by the Romanche Fracture Zone with an offset of about 950 km, and is bordered by a) the Ceará-Potiguar and the East Ghana basin-Togo-Benue conjugate passive margins system and b) the Pará-Maranhão-Barreirinhas and the Deep Ivory Basin-Ghana conjugate passive margins system. These basins, including a divergent margins system with two large parts of strike-slip borders (Campan, 1995; Basile, et al., 2005; Moulin, et al., 2010; Tavares et al., 2020), present a pull-apart configuration.

The extension of the São Luís Craton and its crustal thickness still remain poorly known; few data are present onshore NW Brazil and the closest crustal thickness measurements to the studied area shows an average crustal thickness of 32-36 km (Assumpção, et al., 2013). Due to the lack of deep crustal information, a number of questions remain unanswered on both conjugate margins:: How large is the necking zone? What are the nature and the morphology of the intermediate crustal domain? Are there lateral crustal variations? Is there an asymmetry between the two passive margins? Where is the first oceanic crust located? With a dense set of combined Multi-Chanel (MCS) and wide-angle seismic profiles, the MAGIC (Margins of brAzil, Ghana and

Ivory Coast) deep seismic experiment aims to fill this gap, and, for the first time, to explore the crustal geometry, segmentation and lateral variations of a typical pull-apart margin.
This paper focuses on the divergent component and flow line oriented segmentation of this pull-apart system through two combined MCS and wide angle seismic profiles.

2 Previous data

Studies based on seismic refraction were published in the 1990's on the Ghana-Ivory Coast conjugate margins from EQUAREF, EQUASIS (Basile et al., 1993; Mascle et al., 1995; Sage, 1994; Sage et al., 1997), RRS Charles Darwin Cruise 55 (Pierce et al., 1996; Edwards et al., 1997), IODP leg 159 (Mascle et al., 1988). Nevertheless, the goal of these seismic experiments was not focused to the pull-apart Ghana-Ivory Coast (GIC) segment: they mostly concern the southern strike-slip boundary of the system, where the layered continental crust never exceeds 20 km of thickness, thins abruptly, perpendicularly to the flow lines, across the GIC Ridge, which separates this domain from the oceanic crust southwards.
Few published depth information exists on the conjugate North Brazilian margins. Old existing boreholes and multichannel seismic lines show that the Precambrian basement lies at ~ 2 km depth below the seafloor in the Ilha da Santana Platform. Eastward of the continental shelf the top of the basement deepens very abruptly (Gouyet, 1988). In the early 90's, based on one multi-channel seismic profile and gravity modelling, Azevedo (1991) interpreted a succession of deep reflectors lying at 30-35 km depth below the Ilha da Santana Platform as seismic Moho discontinuity. In the Pará-Maranhão-Barreirinhas basin, Henry et al. (2011) proposed a 15 km thick sedimentary succession and a sharp transition between the continental and oceanic crust. The Pará-Maranhão-Barreirinhas Basin was however covered by the unpublished ION-GXT profiles. Thanks to our collaboration with Petrobras, we added access to them and their analysis shows a segmentation from west to east, with four different main domains (Figure 1B and 1C):
A necking zone of probably continental crust. The Ilha de Santana Platform exhibits a very thin sedimentary cover (~2 km), according to the wells described by Gouyet (1988). The thickness of the basement may be approximatively 22 km. The crust seems to thin very abruptly towards the East, with a basement at 14 km depth and a possible Moho lying at 18km, from which a thickness of 4km is inferred for the crust.
Basin II is characterized by an about 12km-thick sedimentary basin, with probable volcanic interbedded layers. The basement raises seawards from 14 km to 10 km and the depocenter is shifted to the western part, close to the necking domain. No seismic Moho nor deep crustal reflections are observed below this basin.
Basin I coincides with a smaller basin, about 9 km thick, with a possible flower structure, a flat horizontal substratum, and some deep (between 13 and 17 km) and intra-crustal reflectors. No Moho is observed below this domain, except perhaps in the eastern part where some strong dome-shaped reflectors are observed.
The most eastern-ward domain seems of oceanic type. The transition with the previous domain is very sharp. Two series of very strong deep reflectors are observed. The first series of deep reflectors with a roughly flat geometry are located at about 12 km depth, 4 km below what seems to be the top of the basement. The second series of deep reflectors appear to rise eastwards from a depth of 20 km to circa 14 km at the basin depocenter. Depending on which reflectors series is supposed to image the Moho, the proto-oceanic to oceanic domain would therefore represent either a very thinned atypical oceanic crust or an atypical 12km-thick oceanic crust decreasing seawards to a more common 7km-thick one.

3 *The* MAGIC *experiment*

The **MAGIC** (**M**argins of br**A**zil, **G**hana and **I**vory **C**oast) research experiment is a joint

project of the Department of Marine Geosciences (IFREMER: Institut Français de Recherche pour l'Exploitation de la MER, France), the Laboratory of Oceanic Geosciences (IUEM: Institut Universitaire et Européen de la Mer, France), the Faculdade de Ciências da Universidade de Lisboa (IDL, Portugal), the Universidade de Brasilia (Brazil) and PETROBRAS (Brazil). The MAGIC survey was conducted first on the Brazilian side in order to verify the segmentation of the Pará-Maranhão basin and to determine the crustal nature of its domains.

The IFREMER's Marine Geosciences Dep. OBS (Ocean Bottom Seismometer) pool (OldOBS and MicrOBS instruments) was used for offshore wide-angle acquisition. Each OBS is equipped with a three-component geophone and hydrophone. Onshore, portable seismic stations (Reftex 125A-01 acquisition system and seismic sensor L-4C) from the Brazilian Geophysics instrument pool (Observatório Nacional, Rio de Janeiro) were used to record the airgun shots of the R/V *Pourquoi Pas?*. The seismic source consisted of a 7589 in3 array of 18 airguns, towed 25 m below the sea level and fired every 60 s. Shots were also recorded by a 4.5 km long, 360-channel solid streamer towed at 12-15 m depth, 275 m behind the ship. During the MAGIC seismic cruise, 143 Ocean Bottom Seismometers (OBS), a 4.5 seismic streamer and 50 land-stations were deployed along 5 profiles at sea and on-land. Bathymetry, Chirp, multi-channel seismic (MCS) and wide-angle data were acquired on the 5 profiles (MC1, 332 km, MC2, 203 km, MC3, 404 km, MC4, 268 km and MC5, 528 km) between August and October 2012 by the French R/V *Pourquoi Pas?*. Additionally, six cores and one piezometer were deployed during the experiment.

This paper presents the two east-west profiles, acquired parallel to the flow-lines and the fracture zones (MC2 and MC3 profiles, Figure 1). The 400 km-long MC3 profile was shot parallel to the multi-channel seismic ION-GXT 7000 profile from the MC3OBS01 to MC3OBS13. West of this position, the ION-GXT 7000 line deviates towards the South, inducing a maximum distance between to two profiles of ~25 km close to the Ilha de Santana Platform. At sea, a total of 31 OBS were deployed, spaced every 7 nmi. Inland, the profile was extended 220 km towards the West with the deployment of 8 land stations (MC3LSS07 was stolen during the MAGIC experiment). Shots were acquired from MC3OBS01 until MC3OBS29 where water depth shallows to less than 100 m.

On the MC2 profile, a total of 25 OBS were deployed (Figure 1-B). Shots were acquired from MC2OBS01 until MC2OBS25. Note that the geophone channels of MC2OBS12 have malfunctioned during about half of the recording time, possibly due to a bad connection. The geophone of MC2OBS08 was badly coupled to the seafloor resulting in a high noise level.

4 *Multi-channel seismic data*

The MAGIC Multi-Channel Seismic (MCS) data were processed with the Geocluster (CGG-Veritas) software. The processing sequence is composed of: geometry, bandpass filtering (2-8-64-92 Hz), wave-equation multiple attenuation, shot-gather predictive deconvolution, time variant band-pass filter, random multiple attenuation, normal move-out, CMP stack et post-stack FK time migration. During the project MAGIC, some deep multi-channel seismic acquired along ION-GXT profiles (e.g. ION-GXT 7000 Figure 1) have been supplied. These data, combined with the gravimetric map permit to propose a first structural interpretation of the Pará-Maranhão/Barreirinhas margin (Figure 1).

Although the MAGIC multi-channel seismic profiles are less penetrating than the ION-GXT lines, the same structural domains could be identified (Fig 2). Directly East of the Ilha de

Santana Platform, the signal only penetrates the superficial sediments. This allows almost no imaging of the sedimentary record in the continental slope. Directly at the foot of the slope, a ~ 5 to 5.5s twt thick and well stratified sedimentary succession is deposited in Basin II. A good signal is recorded till ~6-7 s twt, with the imaging of a series of stratified and low frequency reflectors. On the MC3 profile, the seismic character becomes quasi transparent below 7 s twt, only few low amplitude reflectors are imaged. Due to low resolution, the top of the basement is sometimes difficult to interpret on the MAGIC seismic profiles. However on the MC2 seismic profile, it seems to lie at 9 s twt in the centre of Basin II (Figure 2). Directly East of the crossing with the MC5 profile, a clear West down-dipping reflector at 8.5 s twt images an abrupt rise of the basement. Beneath the presumed oceanic basin, the top of the basement becomes rough and its depth decreases progressively from 8.5 s twt to ~7.0 s twt. In the presumed oceanic basin, low amplitude and frequency reflectors at 8 s twt are interpreted as the top of the basement. Below the basement is almost transparent with some disrupted reflectors. The deepest main interfaces are interpreted from the MAGIC seismic wide-angle data.

5 *Wide-angle seismic data processing*

All OBSs were relocated by minimizing the difference between the measured direct arrival time of the water wave and the arrival time based on the theoretical, symmetrical water wave hyperbolic arrival. A constant velocity (1510 m/s) in the water layer was assumed and average errors obtained were less than 20 ms. First arrival picking was made without any signal filtering or enhancement to keep the first arrival time unchanged. The picking uncertainty, for other primary and secondary arrivals, is related to the source characteristics but also to attenuation and propagation effects (the shot–receiver distance). It is estimated to be equal to 50–100 ms for all arrivals except the water arrivals, for which the picking uncertainty is less than 10 ms.

Wide-angle plots from Figure 3 to Figure 10 are presented with a reduction velocity of 8 km/s for the land seismic stations and 7 km/s for the OBS records. Amplitude scale is proportional to the offset or its square in order to enhance large-offset arrivals and compensate for geometrical spreading. The distance along profile has the location of the westernmost-OBS as origin.

5.1 Land seismic stations and OBS deployed along the MC3 profile

The MC3 Land Seismic Stations (LSS) allow to image to deep crustal structure below the São Luís Craton and the Ilha de Santana Platform (Figure 1). However the signal on the records is very poor mainly due first to the deployment of these LSS is in a marshy area and secondly to the large offset distance between the LSS and the air gun shots offshore along the MC3 profile. The data show essentially a clear mantle arrival (Pn) between offset of 220 to 430 km and at shorter offset some crustal reflections (Figure 3). Reduced with a velocity of 8 km/s, the MC3 land stations show low amplitude arrivals at 7-7.5 s and a second series of strong and high amplitude arrivals with a delay of 4 s from the low amplitude arrivals, recorded between 11-11.5 s on all the LSS (Figure 3). No refracted phase in the upper continental crust (Pg0) is recorded by the land stations due to their very far offset with the shooting. The termination of Pg1 branch and of Pg1P (refracted and reflected arrivals in the middle continental crust) arrives coincident at 10.5 s, and is modelled with velocities of 6.25 to 6.35 km/s. A weak termination of Pg2 branch (refracted arrival in the lower continental crust) arrives at 9.5 s, associated with velocities of 6.8 to 6.95 km/s (Figure 3). Two mantle arrivals are registered on the land stations, a first arrival refracted Pn1 that propagates with 8.05 to 8.2 km/s between 220 and 430 km offset (Figure 3) and a second arrival Pn2 recorded at very large offset (330 to 430 km) associated with a velocity of 8.2-8.5 km/s (Figure 4). The

MC3 Ocean Bottom Seismometers (OBS) located directly east of the Ilha de Santana Platform east of the continental slope clearly show a thick sedimentary succession with a continuous trend of increasing velocities from 1.8-1.9 km/s to 4.8-5.4 km/s (Figure 5). We identify turning waves from the basement at offset of 30-35 km (Pg2 phase) towards the east, associated with a strong and high amplitude reflected arrivals PuP (Figure 5). Turning waves from the underlying layer (Pu phase – 7.3-7.6 km/s) are observed as first arrivals between offsets of 35 km to 55 km (Figure 5). At larger offset, a clear refracted Pn1 from the mantle is recorded between 50 to 80 km associated with velocities of 8.0 to 8.2 km/s (Figure 5).

Towards Basin II (Figure 2), 7 sedimentary layers are identified on the MC3 OBS's. Between 0 to 70 km model distance, the sedimentary succession presents a continuous trend of increasing P- waves velocities from 1.9 (Ps1) to 5.2 km/s (Ps7) (Figure 5). From 70 km to 180 km model distance, the trend become discontinuous (Figure 6). First sedimentary arrivals refracted phase Ps5 clearly show abrupt increasing velocities in the S5 layer from 3.9-4.0 km/s to 4.35-4.6 km/s (green lines – Figure 6). Below the clear high amplitude refracted Ps5, the S6 layer is characterized by lower velocity of 4.2-4.4 km/s. This velocity inversion is imaged by a step back on the MC3OBS23 to MC3OBS15 records (Figure 6). Below the layer S6, the first arrival Ps7 in the offset range ~22-28 km is a low amplitude phase with apparent velocity of ~5.0-5.3 km/s, and a delay time of ~0.5 s twt relative to the precedent first arrival Ps5. This phase, which propagates in the 7th layer, corresponds to the deepest sedimentary layer S7 with velocities of 4.9-5.2 km/s (Figure 6). On the seismic reflection MAGIC3 profile, the top of the acoustic basement is unclear beneath the Basin II (Figure 2). A clear Pg2 first arrival refracted phase from the crust (B2 layer) is recorded between 20 and 40 km offset, associated with velocities of 6.1-6.9 km/s (light blue – Figure 6). The top of the underlying layer (Pu) is well-imaged on the OBS records with the high-amplitude reflection PuP at offset 20 to 30 km (Figure 6). The refracted phase Pu is a strong and high amplitude first arrival, with velocities of 7.3-7.6 km/s (Figure 6). The base of this layer is marked by a clear and strong reflection Pm1P observed at large offsets (Figure 6). The Moho refracted Pn1 propagates between 50 to 80 km offset, with an apparent velocity of 8.1- 8.2 km/s (Figure 6). On some MC3 OBS, a discontinuous reflected phase with high amplitude and tangent to the Pn1 is observed at large offset (< 45 km) (red phase - Figure 6). It corresponds to deep intra-mantle reflector Pm2P. The velocities of the underlying mantle (Pn2 of 8.2-8.5 km/s) is constrained by the MC3 land station records (Figure 4). East of the MC3OBS13, the high velocity layer S5 and the underlying velocity inversion (layer S6) are not observed (Figure 7). The velocity increases gradually from 1.8-1.9 to 5.1-5.3 km/s. The secondary refracted and reflected arrivals of the layer S6 and S7 are recorded at 15 and 25 km, respectively. The arrivals Ps6 and Ps7 are overlain by the high amplitude Pg2 crustal arrival (Figure 7). The basement arrivals are identified at ~20-30 km offset with apparent velocities close to 6.3-7.0 km/s (layer B2). At ~30 km offset the first arrivals Pu have apparent velocity of 7.6-7.85 km/s decreasing towards the east to 7.5-7.6 km/s, followed by the Pn1 branch with higher velocities of 8.1-8.2 km/s (Figure 7).

Below the presumed oceanic basin from the MC3OBS10 to MC3OBS01 six to five sedimentary layers are observed (Figure 8). Oceanward, the velocities decrease at the base of the sedimentary section from 4.6-5.0 km/s (Ps6) to 4.0-4.2 km/s (Ps5). At the eastern end of the MC3 profile, the MCS data image the rough top of the acoustic basement lying at ~8 s twt (Figure 2). On the MC3 OBS, the presence of a thin intra-crustal layer (B1) is required to explain the arrival-times from the underlying B2 crustal layer. Strong variations of the P-wave velocity occur in the B1 layer (Pg1) and are necessary to correctly model the MC3 OBS's. The Pg1 is a secondary arrival at ~15-25 km offset with apparent velocities decreasing towards the east from 5.8-6.0 km/s to 4.8-5.1 km/s (Figure 8). The Pg2 is a first high

amplitude arrival between 10 and 25 km offset with higher velocities of 6.3-7.0 km/s and the reflected from the crust-mantle interface Pm1P is strong (Figure 8). The Pn1 is observed at maximum offset of 90 km, with velocity within the upper mantle of 8.20 to 8.30 km/s (Figure 8). Although the ION-GXT 7000 profile clearly images a second series of deep reflectors (Figure 1-C), on the MC3OBS records, no more deep intra-crustal reflected phases are observed. However, this second series of deep reflectors corresponds to the prolongation towards the ocean of the deep intra-mantle reflector (Pm2P), recorded by the OBS located in the Basins I and II (Figure 6).

5.2 OBS deployed along the MC2 profile

Below the Basin II, 7 sedimentary layers are identified (Figure 2). Between 20 to 90 km model distance, the sedimentary succession presents a continuous trend of increasing velocities from 1.9 (Ps1) to 5.2 km/s (Ps7). Secondary refracted arrivals close to the water cone allow to constrain velocity in this first sedimentary layer Ps1. They range from 1.88 to 1.92 km/s (dark orange refracted phases – Figure 2). The refracted phase from the second sedimentary layer, Ps2 is a first arrival and is identified up to 15-20 km offset, with apparent velocities that ranges from 2.3 to 2.5 km/s (yellow refracted phases – Figure 9). In the third layer, the first arrival refracted phase Ps3 has apparent velocities of ~3.0-3.3 km/s. The refracted phase Ps4 is a secondary arrival, associated with velocities of ~3.40-3.8 km/s (light green - Figure 2). Although unclear on the OBS sections, presence of this thin S4 layer is required to fit well the arrival times of the underlining layer (green lines - Figure 2). The refracted phase Ps5 is a strong first arrival that is identified up to offsets of ~30 km (green lines - Figure 2). The refracted phases in the 6th and 7th layers are difficult to identify, whereas very clear reflected phases Ps6P and Ps7P are recorded on the OBS's, that allow a good constraint on the base of Basin II. From 90 km to 220 km model distance, this trend becomes discontinuous. First arrival refracted phase Ps5 clearly shows an abrupt increase of the velocities in the S5 layer from 3.9-4.0 km/s to 4.35-4.6 km/s. Below the clear high amplitude refracted phase Ps5, the S6 layer is characterized by lower velocity of 4.2- 4.4 km/s. This velocity inversion is imaged by a step back on the MC2OBS08 to MC2OBS15 records (Figure 2). Below the layer S6, the first arrival Ps7 in the offset range ~22-28 km is a low amplitude phase with apparent velocities of ~5.0-5.3 km/s, and a delay time of ~0.5 s twt relative to the precedent first arrival Ps5. This phase, which propagates in the 7th layer, corresponds to the deepest sedimentary layer imaged on the MCS (Figure 2).

On the MC2 seismic reflection profile, the top of the acoustic basement beneath Basin II is unclear (Figure 2). On the MC2 OBS records, however, the basement and mantle refractions are well-registered till very large offset of 60 to 80 km (Figure 9). A clear first arrival refracted phase Pg1 from the basement is recorded between 20 and 40 km offset, associated with top velocities ranging from 6.0 to 6.3 km/s and bottom velocities from 6.6 to 7.1 km (light blue – Figure 9). The top of the underlying layer (Pu) is well-imaged on some OBS records with the high-amplitude reflection PuP at offset of 20 to 30 km (Figure 9). The first arrival refracted phase Pu is a high amplitude phase with velocities decreasing towards the east from 7.5-7.8 km/s to 7.3-7.6 km/s (Figure 9). The base of this layer is also marked by a clear and strong reflection Pm1P observed at larger offset (Figure 9). The low amplitude mantle refracted Pn1 propagates between 50 to 80 km offset, with an apparent velocity of 8.0-8.5 km/s (Figure 9).

In the oceanic domain, only 6 sedimentary layers have been identified on the MCS data, and correspond to the first 6 sedimentary layers described in Basin II. On the MC2 OBS records, no indication of a relatively high velocity layer S5 is still present (Figure 10). So the sedimentary succession presents a continuous trend of increasing velocities:

- layer S1 with P velocity ranging from 1.88 to 1.95 km/s (Ps1),
- layer S2 with velocity increasing from 2.5 to 2.85 km/s (Ps2),
- layer S3, the velocity of this layer clearly decreases towards the east from 3.0-3.5 to 2.8-2.9 km/s (Ps3),
- layer S4, contrary to Basin II, arrivals appear as a first phase, characterized by a velocity of 3.3-3.8 km/s (Ps4),
- layer S5, arrivals appear as a secondary phase (3.9-4.2 km/s – Ps5) and identification of the refracted phase Ps5 is really ambiguous, due to the difficulty to discriminate this refracted phase from Ps4.
- layer S6, picking of these arrivals is tricky, since the S6 refracted phase is tangent to the S6 reflected phase. The velocity of layer S6 ranges from 4.6 to 5.0 km/s (Ps6). Presence of this layer is required to correctly predict the time arrivals of the underlying crustal refracted phase (Pg1).

The Pg corresponds to a clear arrival at 15 to 30 km offset range. A long and strong Pm1P reflected phase at the crust-mantle boundary is observed on the MC2OBS19 to MC2OBS25 (Figure 10). The triplication point between the Pg1, Pm1P and Pn1 occurs at offset of 30 km, inducing a very thin (5 km) modelled crust with P velocities ranging from 6.3 to 7.2 km/s. In this domain, the very long strong Pm1P recorded between offset of -15 and -80 km (MC2OBS24) is partly explained by the model. In fact, the rays tracing only predict arrivals between-15 and 45 km offset. Pn1 phases propagating towards the east is only visible between 30 to 55 km offset associated with velocities of 8.0-8.1 to 8.5 km/s.

6 Modelling

6.1 Modelling strategy

For phase identification and picking, we have used the interactive plotting software xpicker, available in the Seismic Unix package (Cohen and Stockwell Jr., 2003). We worked upon reduced time record sections, in order to flatten the successive arrivals. The main objective of applying an offset/velocity reduction of times is to horizontalise specific phases, in order to highlight its lateral coherency. We therefore applied reduction velocity that range from 2 km/s to 8 km/s, depending on the apparent velocity of each seismic phase. The data were modelled using an iterative procedure of two-dimensional forward ray-tracing followed by a damped least-squares travel-time inversion from the RAYINVR software (Zelt and Ellis, 1988; Zelt and Smith, 1992). The wide-angle modelling proceeded in a top-to-down strategy of arrival time fitting of the reflected and refracted phases identified in the sedimentary section. For each sedimentary sequence we correlate the twt of its base, from the MCS section, with the arrival times of the reflected and refracted phases identified in the OBS data. An iterative procedure of velocity and depth adjustment, with check of the depth-twt conversion against MCS data was then applied. In the basement we used only the arrival times from the OBS and LSS data set. In order to constrain the velocity gradients of the different layers, synthetic seismograms were calculated and compared to the data sections.

..6.1 The final velocity MC2 and MC3 models

The final velocity models of MC2 and MC3 profiles image the geometry of all sedimentary and crustal layers to a depth of about 55 km (Figure 11). According to the interpretation of the wide-angle data, the velocity structure was modelled using five to seven layers of sediments. Deeper, the crust is modelled with one to three units, and an undefined deeper layer is present beneath the deep Basin II east of the continental slope. Finally, two mantle layers could be distinguished from the MC3 land stations. In the continental domain, between -200 and 0 km model distance of MC3 model, the crustal structure of the São Luís Craton and the Ilha de

Santana Platform is constrained by the MC3 land stations, with the identification of 3 crustal layers: an upper continental crust, with velocity of 6.05 to 6.15 km/s, a middle continental crust with velocity of 6.25 to 6.35 km/s; and a lower continental layer with velocity of 6.8 to 6.95 km/s. The modelled thickness of the continental crust is around 32-33 km. Towards the east, at the foot of the continental slope, seven sedimentary layers are deposited in Basin II. They present a continuous trend of increasing seismic velocities from 1.8-1.9 km/s to 4.9-5.2 km/s. Eastward between 80 and 250 km, the velocity of the 5th layer of the sedimentary column strongly increases to reach 5.05-5.15 km/s on the MC3 profile and 4.5-4.6 km/s on MC2 profile. Presence of this high velocity layer (S5) within the sedimentary piles induces a velocity inversion, within the 6th layer (4.1-4.3 km/s). The total thickness of these first six sedimentary layers is relatively constant ~7 km. The thickness of the 7th sedimentary layer is variable, it progressively decreases towards to the ocean (within the Basin I). The base of the Basin II is marked by a flat interface at 13 km depth, that corresponds to the top of the basement. The modelling results is one-layer crust with a velocity of 6.1-6.7 km/s. This interface becomes rough beneath the Basin I and the velocity of the crust slightly increases to reach 6.3-6.8 km/s. The Basin I domain corresponds to a sharp rise of the basement from 13 km west of the Basin I to 9 km, over a distance of 70 km. Beneath these two Basins II and I, a deep, 3 km thick anomalous velocity layer (AVL) underlies the basement (7.4-7.8 km/s). In the oceanic basin, no high velocities are modelled. The thickness of the sedimentary column is relatively constant ~ 5.5 km with velocity gradually increasing from 1.85-1.95 to 4.5-4.7 km/s. Beneath this sedimentary record, the top of the basement lies at 8 km depth. On the MC3 model, the 5 km thick crustal basement comprised two layers: first a very thin layer 1 km thick with velocity strongly decreasing oceanward from 5.8-6.0 km/s to 4.8-5.1 km/s; second a 4 km thick oceanic layer with velocity of 6.3-7.0 km/s. In contrast, the MC2 model comprises only one crustal layer with velocities increasing toward the east from 6.2-6.6 km/s to 6.4-7.2 km/s. The thickness of this crustal layer increases also towards the east from 3 to 5 km. All along the model, the modelled mantle is characterized by smoothly increasing velocity towards the east from 8.05-8.5 to 8.2-8.5 km/s. Presence of the MC3 LSS allows modelling of an intra-mantle interface lying at depth that was already imaged on the ION-GXT 7000 profiles.

6.2 Travel time fit and model evaluations

The fit between the model and the travel-time picks is given by the root-mean square (RMS). The number of picks, the picking error, the values for the $\chi 2$ parameter and the RMS misfit for each phase are given in Tables 1 and 2. A final velocity model should adequately fit the data predicting arrival-times within the data error bounds, ideally with $\chi 2 = 1$. If $\chi 2 < 1$ the data is over-fit and if $\chi 2 > 1$ the data is under-fit (Zelt and Smith, 1992). However, in practice final $\chi 2$ values significantly different from 1 are often obtained in travel-time inversion (Zelt and Forsyth, 1994). Additional information about the quality of the velocity model can be gained from the resolution parameter (Zelt and Smith, 1992). Resolution is a measure of the number of rays passing through a region of the model constrained by a particular velocity node. As the method of Zelt & Smith (1992) uses a sparsely parametrized inversion, the resolution depends on the node spacing. If a layer can be modelled with one single velocity gradient, the resolution parameter will be high even in areas which have lower ray coverage, since the area is related to only one velocity node. The advantage of this representation is that it allows an assessment of whether all lateral velocity changes are required by the data. Typically, resolution matrix diagonals greater than 0.5–0.7 are said to indicate reasonably well-resolved model parameters (Lutter and Nowack, 1990). The major part of the interface and velocity nodes present very good resolution (> 0.9) (Figure 12)

Synthetic seismograms were also computed to validate modelling as it proceeded. They are

shown on each figure of the MAGIC OBS/LSS to ensure the reader of the accuracy of the P-wave velocities models obtained. Besides modelling of arrival time and amplitude, gravity fit needs to be considered in order to verify the consistency of a velocity model with the mass distribution imprint, since P-wave velocity is directly related to density (lithology, rheological properties, fracturing, pore pressure, etc, have a second order contribution to P-wave velocity). Gravity modelling is performed to evaluate the consistency of the velocity model with the satellite altimeter gravity data and the land data available at the BGI (http://bgi.omp.obs-mip.fr/) (The International Gravimetric Bureau". In: IAG Geodesist's Handbook). A 2-D model consisting of homogeneous density blocks was constructed from the seismic velocity model: in the basement and basins, the seismic velocities are converted to densities according to Ludwig et al. (1970), resulting in densities ranging from 2200 to 2800 kg/m3. The mantle density is set to 3300 kg/m3, and the modelled free-air anomaly is compared to that observed along the profiles. Free air gravity extracted along the MC3 profile presents value comprised between 0 and 50 mGal in the São Luís Craton (red point on Figure 13). Approaching the continental slope towards the east, close to the eastern end of the Ilha de Santana Platform, both the MC2 and MC3 profiles cross the well-known free-air border anomaly with a pick in the free air gravity reaching ~80 mGal. Although the free air border anomaly is not explained by conversion of the MC3 model, the forward model explains generally well (within less than 30 mGal) the observed free air anomaly. Oceanward free air gravity is constant around -20/-30 mGal on both profiles. Series of W-E oriented profiles extracted south and north parallel to MC3 (yellow lines on Figure 13) confirm this trend in the variation of the free gravity from the São Luís Craton to the ocean. Profiles extracted parallel to the MC2 show the same trend of the free air gravity, except at the position 150 km, where a high free air anomaly is recorded, reaching 150 mGal. It is linked with the NW-SE oriented volcanoes, north of the MC2 profile.

7 Discussion on the crustal nature segmentation of the Pará-Maranhão/Barreirinhas passive margin

Velocity-depth profiles below the basement (1D-Vz) were extracted from the model at 10 km interval (Figure 14). The abrupt evolution of these 1D-Vz profiles indicates the existence of five main areas from west to east: the São Luis continental margin, the Ilha de Santana Platform necking domain, a deep basin domain including Basins II and I, and then, in the presumed oceanic area deduced from the analysis of industrial profiles, two sensibly different domains..

I**n the São Luis margin**, the 32-33 km thick continental crust is laterally homogenous in velocity structure, and presents 3 layers with low velocity gradients. Two small velocity steps mark the transition between the upper and middle continental crusts at ~9 km and between the middle and the lower crusts at ~24 km depth. Although it was necessary for modelling to include these 3 layers, the depth of the boundary between the upper and middle continental crusts is poorly constrained. At depth of 32-33 km, the large step where the velocity reaches 8km/s is associated to the Moho. The comparison of the 1D velocity profiles with a worldwide compilation of the continental crust (Christensen and Mooney, 1995) clearly shows similarities both in velocities and gradients (Figure 14). Furthermore, the results obtained for the structure and thickness of the continental crust of the São Luis margin are in agreement with the compilation of seismologic data (Assumpção et al., 2013).

Below the Ilha de Santana Platform, between -50km and 10km model distance, the crust thins abruptly to a thickness of less than 8km in less than 60km.

The three-layered continental crust beneath Ilha de Santana Platform is poorly illuminated, especially the upper crust (Figure 11). However, the model shows that the seismic Moho rises from 33 km to less than 10 km in about 60 km. Taking into account the extension of the Ilha de Santana Platform mapped by Gouyet (1988), based on seismic profiles, drill holes and the isopach maps of the basement available on the GeoBank Brazil (www.cprm.gov.br, Figure 15), we are able to set the geometry of the top of the continental crust, with the top of the basement deepening from 0 to 10 km, whilst the Moho rises from 32-33 km to ~15 km beneath the Ilha de Santana Platform necking domain.

A width similar to the one documented for the Platform Ilha de Santana necking domain has been documented also in other passive margins: 50 km on the Angolan margin (Contrucci et al., 2004a; Moulin, et al., 2005; Aslanian et al., 2009), 100 km in the southern Morocco (Contrucci et al., 2004b; Klingelhoefer et al., 2009; Labails et al., 2009), ~100 km on the Santos margin (Evain et al., 2015), 50 to 100 km in the Western Mediterranean sea (Moulin et al., 2015; Afilhado et al. 2015), <60 km south of the Natal Valley, in the Indian Ocean (Moulin et al., 2020).

The 1D-Vz profiles show clearly the very sharp thinning of the upper continental crust (B0) decreasing from 8 to 0 km in less than 60 km, giving way to the exhumation of middle continental crust (B1) at the toe of the continental slope (Figure 14). The rapid thinning of the middle continental crust gives way, in the deep basin, to the exhumation of the lower continental crust characterized by very high seismic velocity (higher than normal upper continental crust or oceanic crust), up to 6.5 km/s, and a strong velocity gradient.

The deep basin domain (includes Basins II and I).

In the deep basin domain, the upper velocity of the basement on the 1D-Vz profiles increases abruptly to 6.2km/s due to the lack of layers B0 and B1 (Figure 14). The 1D-Vz profiles then remain laterally homogeneous, and present two well separated layers (B2: ~6.2 km/s to ~6.8 km/s and AVL: 7.3km/s to 7.8 km/s), except for a few thickness variations of the upper layer, between 180 and 200 km model distance. The B2 crustal layer has an average thickness of 3 km, as the AVL, which disappears around 270 km. The differences between the Basins I and II are of secondary importance and represent mainly a change in the roughness of the basement top, a rise of the basement from about 12 to 10 km, and small variations of the thickness of the basement layer. Figure 16 presents the total Velocity/depth profiles (including the water and sedimentary layers) at the crossing points of the MAGIC wide-angle profiles in the deep basin domain, and exhibits a fairly good fit. All the profiles evidence the presence of strong abrupt increase in the sedimentary seismic velocities between 7 and 8 km depths, and an inversion in the underlying layer. This sharp variation of velocity with depth represents a change in sedimentary nature, and is probably due to the presence of a volcano-sedimentary layer of about 1 km of thickness, characterized by a velocity reaching 5 km/s within a sedimentary sequence around 4 km/s. The basement presents on all profiles a 5-6 km thickness, with an upper layer with velocity ranging from 6.2 to 6.6 km/s and a lower layer with very high velocity, in average 7.4-7.6 km/s.

This overall basement thickness of 5-6 km, the very high seismic velocity at the basement top and the presence of an AVL do not fit the continental worldwide compilation (Christensen and Mooney, 1995) nor the typical oceanic compilation (White et al., 1992) (Figure 14).

Figure 17 (A-B-C) compares the 1D-Vz profiles in the basement extracted along the MC2 and MC3 profiles with 1D-Vz profiles extracted from wide-angle seismic models in Iberia

Abyssal Plain (A), Newfoundland Grand Banks margin (B) and the southern Galician margin (C), where exhumed mantle, serpentinised upper mantle, or a mixture of both have been proposed. Serpentinised upper mantle and lower continental crust materials were drilled in the southern Galician margin during Legs 173 and 149 of the Ocean Drilling Program (Chian et al., 1999), the lower continental crust materials being interpreted as rafts that float in an overall upper mantle exhumation regime that occurs along a deep detachment (Boillot et al., 1980, 1988; Manatschal et al., 2001). In the southern Iberian Abyssal Plain, Dean et al. (2000) inferred the presence of 5km-thick exhumed upper mantle divided into two layers (IAM-9 profile). Lastly on the eastern Grand Banks of Newfoundland, van Avendonk et al. (2006) propose the existence of a ~25 km-wide exhumed upper mantle domain (SCREECH-2 profile). In these three areas, 1D-Vz profiles exhibit a continuous increase of velocity with depth and absence of intra-basement interfaces and completely differ from the 1D-Vz of the deep basin of the Pará-Maranhão/Barreirinhas passive margin.

Figures 17-D-E-F-G present a comparison with the 1D-Vz profiles of the transitional domain in the Provençal basin (Moulin et al., 2015 ; Afilhado et al., 2015), in the Jequitinhonha Basin (Loureiro et al., 2018), in the Santos Basin (Evain et al., 2015) and in the Tagus Abyssal Plain (Afilhado et al., 2008). As in the deep basin of Pará-Maranhão/Barreirinhas margin, the velocity structures of these transitional domains exhibit an upper layer with high velocity at the top (from 5,8 to 6,7km/s), a first sharp velocity step, an underlying anomalous velocity layer, and a second sharp velocity step at the base of the lower layer (a strong and well-defined Moho).

In the Gulf of Lion-Provençal basin, the lack of evidence for crustal extension in the upper crust, the prominent inter-crustal T-reflector at the outermost necking on the seismic profiles (De Voogd et al., 1991; Pascal et al., 1993; Bache et al., 2010; Séranne et al., 1995), the high velocities at the top of the basement in the deep basin, the presence of a lower layer with anomalous velocities together with, at its base, a strong velocity contrast and high-amplitude reflectors on the MCS profile, interpreted as the velocity step at the top of the mantle favour the hypothesis of lower crust exhumation along a landward deep detachment (Figures17D; Séranne et al., 1995; Séranne, 1999; Moulin et al., 2015; Jolivet et al., 2020).

Figures17E and 17F present the comparison with the 1D-VZ profiles of the deep basin of the Jequitinhonha basin and the deep domain of the Santos Basin, respectively, interpreted lower continental crust underlain by an anomalous velocity layer (Loureiro et al., 2018) or exhumed middle continental crust (Evain et al., 2015). The anomalous velocities may be interpreted as deriving from intrusions of mantle-derived melts into the lower continental crust (Loureiro et al., 2018) as proposed in the Paleoproterozoic block of the Ukrainian Shield (Thybo et al., 2003; Thybo & Artemieva, 2013) when the lower continental crust started to thin and/or begin to flow (Bott, 1971; Buck et al., 1999; Aslanian et al., 2009). A similar mechanism has also been proposed for the Uruguayan margin (Clerc et al., 2015)

At the Tagus Abyssal Plain (Fig. 17G), the ocean-continent transition zone is marked by two distinct layers with velocities ranging from roughly 6.0- 6.3 km/s and 6.4-7.2 km/s. Modelling the data from this region required two velocity steps, one at the intra-crustal layer boundary and one at the Moho. Both correspond to changes in the reflectivity observed in the MCS data. Based on these findings the authors argue for "*a transitional domain basement composed of thinned continental crust overlying a heterogeneous layer of intruded gabbros or intruded serpentinised peridotites, that vanished below the undoubtedly continental crust in the continental slope*" (Afilhado, et al., 2008). Note that this hypothesis differs completely

from the one proposed less than 100 km to the North on the Iberian Margin (Dean et al., 2000).

The velocity structure of the deep basin of the Pará-Maranhão/Barreirinhas margin is noticeably different from that of profiles where the basement is presumably formed of exhumed mantle (Figures 17 A-B-C). The deep basin of the Pará-Maranhão/Barreirinhas margin has an upper layer with much higher velocities and lower gradients, and clear reflections from the Moho are seen in both wide-angle and near offset seismic sections that are associated with strong velocity contrasts. These differences clearly demonstrate that the basement of the Pará-Maranhão/Barreirinhas deep basin cannot be formed of exhumed mantle. Following the interpretation in the Santos, Jequitinhonha, Provençal and Tagus Basins (Figure 17 D-E-F-G), with a similar velocity profile structure, Moho marker and high velocities, we argue that the deep basement of the Pará-Maranhão/Barreirinhas margin is made of exhumed lower continental crust, showing its crucial role in the Passive margin genesis, as suggested previously by Aslanian et al. (2009) on the Angola Margin. This exhumed lower continental crust overlies an anomalous velocity layer (AVL) which may have resulted from intrusions of mantle-derived melts into the lower continental crust, as suggested in the Tagus (Afilhado et al., 2008), the Angola (Aslanian et al., 2009) and the Jequitinhonha (Loureiro et al., 2018) basins.

Based on MCS seismic profiles only, an **Oceanic Domain** was interpreted eastwards the offshore boundary of the deep basin, marked by aligned volcanoes in the northeastern part (Figure 1),

The 1D-Vz profiles allow to distinguish two sub-domains (Figures 14 & 18-A). Within these two subdomains, the thickness of the basement remains 5 km. Modelling of the MC3OBS allows to constrain the depth of Moho beneath the basement at 12.5 km, which is coherent with the interpretation of the Moho's depth on ION GXT 7000 profile (Figure 1-C, Moulin et al., submitted).

Eastwards of the deep basin and the NW-SE volcanoes alignment, the AVL that underlies the deep basin quite abruptly disappears (blue dash lines in Figure 18A): the westernmost domain A basement (purple lines in Figures 14 & 18-A) is characterized by a 5-km thick single layer with high velocity at the top (5.8-6.0 km/s) and a lower boundary at 6,8-7km/s, marked by a strong velocity step with the upper mantle layer. These characteristics are homogeneous along the MC1 NW-SE profile and show the domain A as a continuous NW-SE strip parallel to the Ilha de Santana coast and to the alignment of the NW-SE volcanoes, in the continuity with the 60 km-wide coastal bend observed in the Borborema region (Moulin et al., submitted). The easternmost domain B basement (red lines in Figures 14 & 18-A) is characterized by two layers: the 1.5km-thick upper layer shows a low velocity gradient (4,8-5,2 km/s) and a very strong step at its bottom. The lowest layer then presents a velocity structure with a lower boundary at 6,8-7km/s, similar to that of the domain A at the same depth, but a lower gradient with the top velocity at 6.4-6.6 km/s instead of 6.1-6.3km/s at the same depth on domain A. Whilst thinner, domain B exhibits 1D-velocity-depth profiles with gradients and velocities coherent with a thin oceanic crust (Figure 14 & 18A). Is it worth to note that, north to São Paulo Fracture Zone, in the Amazon Cone (segment 1 on figure 1), Watts et al. (2009) described a thin oceanic domain with similar velocity structure.

The study of the 1D-Vz profiles of the Pará-Maranhão/Barreirinhas margin's oceanic domain, therefore, shows that the passage between the deep basin and the thin oceanic crust is progressive with two steps (Figure 19): first the deep AVL disappears and the uppermost

basement layer thickens with a very continuous velocity structure compared with the deep basin, then eastward a layer appears on the top of the basement with much lower velocities and the velocity gradient decreases within its lower layer (see Moulin et al., companion paper submitted, for details).

Figure 18-B presents a comparison of 1D basement velocity-depth profiles of the assumed first oceanic crust offshore two conjugate margins of the Provençal Basin, in the Western Mediterranean Sea: the Gulf of Lion (purple lines) and the Sardinia Margin (red lines).
Based on magnetic, gravity maps and seismic profiles, the Liguro-Provençal basin is described as a symmetrical passive margin system, but with a smaller domain in the West Sardinian margin (Bayer et al., 1973; Galdéano & Rossignol, 1977; Rollet et al., 2002; Bache et al., 2010; Gailler et al., 2009; Moulin et al., 2015; Afilhado et al., 2015; Jolivet et al., 2020). The central part of the Liguro-Provençal Basin is characterized by low gravity anomalies and concomitant magnetic anomalies patterns that sharply differ from the magnetically-quiet adjacent domains (Bayer et al., 1973; Galdéano & Rossignol, 1977 ; Leroux et al., 2018). This basin is assumed to be underlain by oceanic crust (Burrus, 1984; Le Douaran et al., 1984; De Voogd et al., 1991; Pascal et al., 1993; Rollet et al., 2002; Gailler et al., 2009), which begun to form in the Late Aquitanian (between 23 and 19 Ma), 9 Ma after a short-lived episode of rifting (Gorini et al., 1993; Mauffret et al., 1995; Séranne, 1999; Guennoc et al., 2000; Bache et al., 2010).

Nevertheless, based on the SARDINIA wide angle experiment data, Moulin et al. (2015) described this domain in the Gulf of Lion as a very thin (only 4-5 km) “atypical” oceanic crust, which, despite its difference in the magnetic signature, presents similar velocities profiles as of the landward located domain (purple 1D-Vz on Figure 18-B) inferred to be made of exhumed lower continental crust (Gailler et al., 2009 ; Moulin et al., 2015).
Then, on the conjugate Sardinian margin, the 1D-Velocity profiles seem to represent a more classical but thinner oceanic crust (Afilhado et al., 2015). This evolution with the setup of an upper layer with lower velocities has strong similarities with the one that we described in the Pará-Maranhão/Barreirinhas margin.

Figure 18C presents the comparison with the 1D-Vz in the central part of the Santos Basin-São Paulo Plateau System (SSSP). In that area, the opening direction is oblique to general opening motions of the South American and African plates (Moulin et al., 2010, 2012) and the SSPP represents an entire conjugate passive margins system, very similar in geometry to the one of the Liguro-Provençal Basin. As in the Liguro-Provençal Basin, the central part of the SSSP exhibits very different magnetic and gravimetric patterns compared to the surrounding domains, with a v-shaped pattern of positive gravity anomalies comprised in a large area of mostly negative magnetic anomalies (Moulin et al., 2012). These are connected with changes in depth of the basement surface and in salt morphology (Evain et al., 2015 ; Bellucci et al., submitted) but are correlated with a heterogeneous crustal structure with a thin to extremely thin crust (Evain et al., 2015). Two series of 1D-Vz are shown, along two parallel profiles separated by 80km, and present therefore the lateral variations that we can observe in such area.
The velocity structure of the southwestern part of the SSPP (Figure 18-C, pink lines) presents two layers with a similarly strong velocity gradient (from 5,5 to 6,8 km/s) and a strong step at the Moho, following the trend of surrounding domains proposed as exhumed middle-lower continental crust. In the northeastern part, the 1-D velocity-depth profiles (Figure 18-C, purple lines) present (1) a much thinner upper layer, with very high velocity and a large velocity step (0.5 km/s) at its base, (2) a continuously increasing velocity up to mantle-like

values (7.8 km/s), and therefore (3) an absence of velocity step at the Moho. Evain et al (2015) concluded that the northeastern part of the central domain of SSPP system could consist either of an upper layer of oceanic nature, but atypical and without its layer 2 (basalt), or of continental nature (with mafic intrusions or exhumed lower crust), and a lower high-velocity layer of intruded lower continental crust or altered mantle. The oceanisation process seems therefore more evolved in the Northern part of the SSPP, which is coherent with the Eulerian pole given by the palinspastic reconstruction (Moulin et al., 2012).

Combining refraction/reflection data together with a detailed kinematic reconstruction, Aslanian et al. (2009, 2012) stated that part of the lower continental crust is still missing in the palinspastic reconstruction of the South Atlantic Ocean and that it seems most improbable that the continental crust maintains its integrity throughout the thinning process. Following the initial idea of Bott (1971), Aslanian et al. (2009) and then Sibuet and Tucholke (2012) suggested that this missing lower crust may have flowed and fed a first atypical oceanic crust. In such a case, the high velocities (7.0–7.8 km/s) in the lower layer of the Santos basin may represent either mantle in an elevated position, altered but not exhumed, or highly intruded lower continental crust. A high-velocity layer without a clearly identified Moho was modelled along several margins (e.g., Newfoundland: Funck et al. (2003); Iberia: Dean et al. (2000); Angola: Contrucci et al. (2004a), Mediterranean Sea: Moulin et al., 2015; Brazilian margins: Loureiro et al., 2018; this article). Many of these studies propose the presence of serpentinized mantle either underlying continental or oceanic crust or simply exposed beneath a sedimentary cover (exhumed). The assumption behind these interpretations is that the thinning process could allow fracturing and create pathways for seawater to reach the mantle and initiate its serpentinization. Such process would then lower mantle velocities.

Conclusions

In the Pará-Maranhão/Barreirinhas passive margin, the wide-angle data reveal a strong E-W-segmentation with (Figures 19 & 20):

- A necking zone corresponding to a very abrupt decrease (about 50 km wide) of the continental thickness from about 35 km to about 10 km; its seaward limit is highlighted by a high on the satellite derived free-air gravity anomalies map.
- An intermediate domain, presenting a 5-7km thick sedimentary sequence, with a volcanic-sedimentary interbedded layer characterised by high seismic velocity. This sedimentary sequence lies on a substratum made of exhumed lower continental crust overlying a layer possibly made of intrusions of mantle-derived melts into the lower continental crust, with an anomalous velocity structure (AVL). The eastern boundary of this intermediate domain is overprinted by the presence of a NW-SE volcanic alignment, parallel to the hinge line, and the disappearance of the AVL.
- The transition to oceanic crust is more complex than expected, with the presence of an about 60 km-wide band of proto-oceanic crust before a “more typical” but still thin oceanic crust eastward. This proto-oceanic crust presents, in its upper part, seismic velocity higher than “normal” oceanic crust but in continuity with the velocity described in the intermediate domain.

Following Bott (1971) and Aslanian *et al.* (2009), we suggest strong crustal interactions at the onset of oceanic crust formation (i.e. proto-oceanic), involving lower continental material flowing that feed a first atypical oceanic crust, as already observed in the Liguro-Provençal basin (Afilhado *et al.,* 2015; Moulin *et al.,* 2015) or in the Santos Basin (Evain *et al.,* 2015).

Based on these observations, we propose that 1) the so-called intermediate domain in Th deep basin is mainly of exhumed middle/lower continental nature, overlying a high velocity layer (HVL) which may be composed of intrusions of mantle-derived melts into the lower continental crust; 2) whilst velocity structures seem to depict a strong segmentation in velocity structure, the passage between an intermediate domain and a typical oceanic crust is not abrupt in terms of composition but takes place in stages, and involves the lower continental crust: the first evolution occurs in the deepest part and produces a domain of proto-oceanic crust made of a highly intruded exhumed lower continental crust; the second stage sets up an upper layer with typical oceanic features.

Acknowledgements

We are indebted to the captain, crew, and MCS technical team of the R/V Pourquoi Pas?. We also thank J. Crozon, P. Pelleau, M. Roudaut, R. Apprioual, D. Le Piver & P. Fernagu (Ifremer), and C. Prunier (IUEM), the OBS technical team, and A. Loureiro, C. Corela, J-L. Duarte, I. Bernardo, D. Alves (IDL - Portugal) and J. Soares, M. V. de Lima (Univ of Brasilia, Brazil), the land stations deployment team. The GMT (**Wessel & Smith 1998**), Seismic Unix (**Stockwell 1999; Cohen and Stockwell, 2015**), and Geocluster (CGG-Veritas) software packages were used extensively in the preparation of this paper. Processing of the high resolution chirp data was done by A. Baltzer, M. Benabdellouahed, and M. Rabineau. The geodynamic interpretations were done by D. Aslanian and M. Moulin. R. Fuck acknowledges CNPq, Brazil research fellowship and INCT Estudos Tectônicos research grant. The authors acknowledge financial support from CAPES-COFECUB.

The dataset collected during the MAGIC experiment is protected under a partnership with Petrobras. Any request has to be addressed to Daniel Aslanian (aslanian@ifremer.fr) and Adriano Viana (aviana@petrobras.com.br).

Contributions

The MAGIC Project was imagined by D. Aslanian and led by D. Aslanian, M. Moulin from Ifremer and A. Viana, Otaviano da Cruz Pessoa Neto from Petrobras. The Onshore part of the project was managed by N. Dias from ISEL (Lisbon), R. Fuck and J. Soares from University of Brasilia. Modelling of the MAGIC profiles was done by M. Moulin, F. Gallais, A. Afilhado and P. Schnurle. Processing of the deep seismic reflection data was done by P. Schnurle. Landstantions were deployed by N. A. Dias, A. Afilhado, A. Loureiro, C. Corela. The Geologic interpretation interpretation were done by D. Aslanian, M. Moulin., P. Schnürle, A. Leprêtre, M. Evain, P. de Clarens, J. Thompson. All co-authors participate to the writing of the paper. The MAGIC Team is composed by: A. Baltzer[6], M. Rabineau[7], Z. Mokkedem[7], M. Benabdelhouahed[7], M. Evain[1], A. Loureiro[3], D. Alves[3], F. Klingelhoefer[1], R. Apprioual[1], J. Crozon[1], P. Fernagu[1], D. Le Piver[1], P. Pelleau[1], C. Prunier[7], M. Roudaut[1], L. Morvan[1], D. Pierre[1], E. Boisson[1], M. Roudaut-Pitel[1], I. Bernardo[3], C. Corela[3], J.L. Duarte[3], M. De Lima[8], L. Matias[3], F. Farias[5], R. Pellen[1,6], B. Pereira[5], C. Rigoti[5] & W. Roest[1].

References

Afilhado, A., Matias, L., Shiobara, H., Hirn, A., Mendes-Victor, L. and Shimamura, H., 2008. From unthinned continent to ocean: The deep structure of the West Iberia passive continental margin at 38°N. Tectonophysics, 458: 9-50.

Afilhado, A. Moulin, M., Aslanian, D., Schnürle, P., Klingelhoefer, F., Rabineau, M., Leroux, E., Beslier, M.-O., 2015, Deep Crustal Structure Across An Young Passive Margin From Wide- Angle And Reflection Seismic Data (The Sardinia Experiment) - II: Sardinia's Margin, Bulletin de la Société Géologique de France, 186, n°4-5, 331-351, doi:10.2113/gssgfbull.186.4-5.331.

Aslanian, D., Moulin, M., Olivet, J-L., Unternehr, P., Bache, F., Rabineau, M., Matias, L., Nouzé, H., Klingelhoefer, F., Contrucci, I. And Labails, C., 2009. Brazilian And African Passive Margins Of The Central Segment Of The South Atlantic Ocean: Kinematic Constraints, Tectonophysics, 468, 98-112.

Assumpção, M., Bianchi, M., Julià, J., Dias, L.D., França, G.S., Nascimento, R., Drouet, S., Pavão, C.G., Albuquerque, D.F. and Lopes, A.E.V., 2013. Crustal thickness map of Brazil: Data compilation and main features. Journal of South American Earth Sciences, 43: 74-85.

Azevedo, R.P., 1991. Interpretation of a Deep Seismic Reflection Profile in the Pará- Maranhão Basin. Congresso Brasileiro de Geofísica, 2, Bol. Res. Exp., Salvador, BA, II, SBGF, Salvador, BA: 661–666.

Bache, F., Olivet, J.-L., Gorini, C., Aslanian, D., Labails, C. & Rabineau, M., 2010. Evolution of rifted continental margins: The case of the Gulf of Lions (Western Mediterranean Basin), Earth and Planetary Science Letters, 292, 345-356.

Basile C, Mascle J, Popoff M, Bouillin JP, Mascle G, 1993. The Ivory Coast-Ghana transform margin: a marginal ridge structure deduced from seismic data. Tectonophysics 222:1–19

Basile, C., Mascle, J. and Guiraud, R., 2005. Phanerozoic geological evolution of the Equatorial Atlantic domain. Journal of African Earth Sciences, 43: 275–282.

Bayer, R., Le Mouel, J.L., Le Pichon, X., 1973. Magnetic anomaly pattern in the western Mediterranean. Earth and Planetary Science Letters, 19 (2), 168-176.

Bellucci M., Aslanian D., Moulin M., Rabineau M, Leroux E., Pellen R., Poort J., Del Ben A., Gorini C., Camerlenghi A., Salt morphologies and crustal segmentation relationship: new insights from well-known salt-bearing margins,submitted to ESR,16 October 2020

Boillot, G., Grimaud, S., Mauffret, A., Mougenot, D., Kornprobst, J., Mergoil-Daniel, J., and Torrent, G., 1980. Ocean-continent boundary off the Iberian margin: a serpentinite diapir west of the Galicia Bank: Earth and Planetary Science letters, v. 48, no. 1, p. 23-34.

Boillot, G., Winterer, E., others, 1988. Drilling on the Galicia Margin: Retrospect and Prospect. In: Proceedings of the Ocean Drilling Program, Scientific Results. Ocean Drilling Program College Station, TX, pp. 809e828.

Bott, M.H.P., 1971. Evolution of young continental margins and formation of shelf basin. Tectonophysics 11, 319–337.

Buck, W.R., Lavier, L.L., Poliakov, A.N.B., 1999. How to make a rift wide. philos. Trans. R. Soc. Lond. Ser. a-Mathematical Phys. Eng. Sci. 357 (1753), 671e690.

Burrus, J., 1984. Contribution to a geodynamic synthesis of the Provenqal Basin (North-Western Mediterranean). Marine Geology, 55, 247-269.

Campan, A., 1995. Analyse cinématique de l'Atlantique Equatorial, implications sur l'évolution de l'Atlantique Sud et sur la frontière de plaque Amérique du Nord/Amérique du Sud. Paris, Université Pierre et Marie Curie, Paris VI. 352 pp.

Chian, D.P., Louden, K.E., Minshull, T.A. & Whitmarsh, R.B., 1999. Deep structure of the ocean-continent transi- tion in the southern Iberia Abyssal Plain from seismic refraction profiles: Ocean Drilling Program (Legs 149 and 173) transect. Journal of Geophysical Research- Solid Earth 104 (B4), 7443-7462.

Christensen, N.I. and Mooney, D.W., 1995. Seismic velocity structure and composition of the continental crust: A global view. Journal of Geophysical Research, 100(B7): 9761-9788.

Clerc C., Jolivet L., Ringenbach J.-C., 2015. Ductile extensional shear zones in the lower crust of a passive margin,Earth and Planetary Science Letters, Volume 431, Pages 1-7, https://doi.org/10.1016/j.epsl.2015.08.038.

Cohen, J.K. and Stockwell Jr., J.W., 2003. CWP/SU: Seismic Unix Release 37: an open source package for seismic research and processing, Center for Wave Phenomenan Colorado School.

Contrucci, I., Matias, L., Moulin, M., Géli, L., Klingelhoefer, F., Nouzé, H., Aslanian, D., Olivet, J.L., Réhault, J.P. and Sibuet, J.C., 2004a. Deep structure of the West African continental margin (Congo, Zaïre, Angola), between 5°S and 8°S, from reflection/refraction seismics and gravity data. Geophysical Journal International, 158: 529-553.

Contrucci, I., Klingelhoefer, F., Perrot, J., Bartolome, R., Gutscher, M.A., Sahabi, M., Malod, J. and Rehault, J.P., 2004b. The crustal structure of the NW Moroccan continental margin from wide-angle and reflection seismic data. Geophysical Journal International, 139: 117–128.

Dean, S.M., Minshull, T.A., Whitmarsh, R.B. and Louden, K.E., 2000. Deep structure of the ocean-continent transition in the southern Iberia Abyssal Plain from seismic refraction profiles' The IAM-9 transect at 40°20'N. Journal of Geophysical Research, 105(B3): 5859-5885.

De Voogd, B., Nicolich, R., Olivet, J.L., Fanucci, F., Burrus, J., Mauffret, A., Pascal, G., Argnani, A., Auzende, J.M., Bernabini, M., Bois, C., Carmignani, L., Fabbri, A., Finetti, I., Galdeano, A., Gorini, C.Y., Labaume, P., Lajat, D., Patriat, P., Pinet, B., Ravat, J., Ricci Luchi, F., Vernassa, S., 1991. First deep seismic reflection transect from the Gulf of Lions to Sardinia (ECORS–CROP profiles in Western Mediterranean), In: Meissner, R., Brown, L., Durbaum, H.-J., Fuchs, K., Seifert, F. (Eds.), Continental Lithosphere: Deep

Seismic Reflections. v. Geodynamics, 22. American Geophysical Union, Washington, pp. 265–274.
Edwards, R. A., Whitmarsh, R. B., and Scrutton, R. A. , 1997. The crustal structure across the transform continental margin off Ghana, eastern equatorial Atlantic, J. Geophys. Res., 102(B1), 747– 772, doi:10.1029/96JB02098.
Evain M., A. Afilhado, C. Rigotti, A. Loureiro, D. Alves, F. Klingelhoefer, P. Schnürle, A. Feld, R. Fuck, J. Soares, M. Vinicius de Lima, C.Corela, L. Matias, M. Benabdellouahed, A. Baltzer, M. Rabineau, A. Viana, M. Moulin, D. Aslanian, (2015): Deep structure of the Santos Basin-São Paulo Plateau System, SE Brazil; J. of Geophy. Res. - Solid earth, doi:10.1002/2014JB011561.
Funck, T., Hopper, J. R., Larsen, H. C., Louden, K. E., Tucholke, B. E., and Holbrook, W. S., 2003, Crustal structure of the ocean-continent transition at Flemish Cap: Seismic refraction results: Journal of Geophysical Research, v. 108, no. B11, p. 2531.
Gailler, A., Klingelhoefer, F., Olivet, J.-L., Aslanian, D. and the Sardinia scientific and technical OBS teams. 2009. Crustal structure of a young margin pair: New results across the Liguro–Provencal Basin from wide-angle seismic tomography, Earth and Planetary Science Letters, 286, 333-345.
Galdeano, A. & Rossignol, J.-C., 1977. Assemblage à altitude constant des cartes d'anomalies magnétiques couvrant l'ensemble du bassin occidental de la Mediterraneée. Bulletin de la Société Géologique de France, 19, 461-468.GeoBank Brazil, http://geobank.sa.cprm.gov.br.
Gorini, C., Le Marrec, A. & Mauffret, A., 1993. Contribution to the structural and sedimentary history of the Gulf of Lions (Western Mediterranean) from the ECORS profiles, industrial seismic profiles and well data. Bull. Soc. géol. Fr., 164, 353–363.
Gouyet, S., 1988. Evolution tectono-sédimentaire des marges guyanaise et Nord-Brésilienne au cours de l'ouverture de l'Atlantique Sud. PhD Thesis, university of Pau et des pays de l'Adour, 374p.
Guennoc, P., Gorini, C. & Mauffret, A., 2000. Histoire géologique du Golfe du Lion et cartographie du rift oligo-aquitanien et de la surface messinienne. Géol. Fr., 3, 67–97.
Heine, C., Zoethout, J., Mueller, R. D., 2013. Kinematics Of The South Atlan- tic Rift, Solid Earth Volume: 4 Issue: 2 Pages: 215-253.
Henry, S., Kumar, N., Danforth, A., Nuttall, P. & Venkatraman, S., 2011. Brazil Equatorial Margin shows Promise. GeoExpro, vol. X, 39-40.
Klingelhoefer, F., Labails, C., Cosquer, E., Rouzo, S., Géli, L., Aslanian, D., Olivet, J.L., Sahabi, M., Nouzé, H. and Unternehr, P., 2009. Crustal structure of the SW Moroccan margin from wide-angle and reflection seismic data (the Dakhla experiment). Tectonophysics, 468(63-82).
Labails, C., Olivet, J.L. and group, T.D.s., 2009. Crustal structure of the SW Moroccan margin from wide-angle and reflection seismic data (the Dakhla experiment). Part B - The tectonic heritage. Tectonophysics, 468: 83-97.
Le Douaran, S., Burrus, J., Avedik, F., 1984. Deep structure of the North-Western Mediterranean basin: results of a two-ship seismic survey, Marine Geology, 55, 325–345.
Leprêtre, A., Verrier, F., Evain, M., Schnurle, P., Aslanian, D., de Clarens, P., Dias, N., Afilhado, A., Gonçalves, S., Moulin, M., and MOZ3/5 Team, Deep structure of the North Natal Valley (Mozambique) using combined wide-angle and reflection seismic data. Journal of Geophysical Research: Solid Earth, 126, e2020JB021171. https://doi.org/10.1029/2020JB021171
Leroux, E., Aslanian, D., Rabineau M., Gorini, C., Rubino, J.-L., Blanpied, C., & Poort, J., Atlas of the Stratigraphic markers in the western Mediterranean sea with focus on the Gulf of Lion, Commission de la Carte Géologique du Monde, 2018
Loureiro, A., Afilhado, A., Matias, L., Moulin, M., Aslanian, D., 2016. Monte Carlo approach to assess the uncertainty of wide-angle layered models: Application to the Santos Basin, Brazil. Tectonophysics, 683, 286– 307. https://doi.org/10.1016/j.tecto.2016.05.040.
Ludwig, W.J., Nafe, J.E. & Drake, C.L., 1970. Seismic refraction, in The Sea, 4, pp. 53-84, ed. Maxwell, A.E., Wiley, New York.
Lutter, W.J. and Nowack, R.L., 1990. Inversion for crustal structure using reflections of the PASSCAL Ouachita experiment. Geophysical Journal International, 95: 4633-4646.
Manatschal, G., Froitzheim, N., Rubenach, M., Turrin, B.D., 2001. The role of detachment faulting in the formation of an ocean-continent transition: insights from the Iberia Abyssal Plain, Geol. Soc. Lond. Spec. Publ. 187 1: 405-428, doi:10.1144/gsl.sp.2001.187.01.20.
Mascle, J., Lohmann, Gp, Clift, P, 1995. The Cote-Divoire Ghana Transform Margin - Preliminary-Results From Odp Leg 159 (January February 1995), Comptes Rendus De L Academie Des Sciences Serie Ii Volume: 320 Issue: 8 Pages: 737-747 Part: 2.
Mascle, J., Lohmann, G.P., Moullade, M., 1998. Proc. ODP, Sci. Results, 159: College Station, TX (Ocean Drilling Program).
Mauffret A, Pascal G, Maillard A, & Gorini C., 1995. Tectonics and deep structure of the north-western Mediterranean Basin. Marine and Petroleum Geology, 12, 645-666.

Moulin, M., Aslanian, D., Olivet, J-L., Contrucci, I., Matias, L., Géli, L., Klin- gelhoeffer, F., Nouzé, H. And. Réhault, J-P & Unternehr, P., 2005. Geological Constraints On The Evolution Of The Angolan Margin Based On Reflection And Refraction Seismic Data Zaïango Project . Geophys. J. Int. 162: 793-810

Moulin, M., Aslanian, D. and Unternehr, P., 2010. A new starting point for the South and Equatorial Atlantic Ocean. Earth-Sciences Review, 98: 1-37.

Moulin, M., Aslanian, D., Rabineau, M., Patriat M., &Matias, L., Kinematic Keys of the Santos - Namibe Basins, In: Mohriak, W.U., Danforth, A., Post, P.J., Brown, D.E., Tari, G.C., Nemcok, M. & Sinha, S.T. (eds). Conjugate Divergent Margins. Geological Society, London, Special Publications, 369, http://dx.doi.org/10.1144/SP369.3. 2012

Moulin M., Klingelhoefer F., Afilhado A., Aslanian D., Schnurle P., Nouzé H., Rabineau M., Beslier M.O., & Feld A., 2015. Deep Crustal Structure Across An Young Passive Margin From Wide- Angle And Reflection Seismic Data (The Sardinia Experiment) - I. Gulf Of Lion's Margin, Bulletin de la Société Géologique de France, 186, n°4-5, 309- 330, doi:10.2113/gssgfbull.186.4-5.309.

Moulin, M., Aslanian, D., Evain, M., Leprêtre, A., Schnurle, P., Verrier, F., Thompson, J., De Clarens, P., Dias, and the PAMELA-MOZ35 team, Gondwana breakup and passive margin genesis: Messages from the Natal Valley, Terra Nova, 32:205–214. 2020. https://doi.org/10.1111/ter.12448

Moulin M., Gallais F., Afilhado A., Schnurle P., Dias N., Soares J., Fuck R., Viana A., Aslanian D. & MAGIC Team. Image of a first oceanic crust in the Equatorial Atlantic Ocean: insights from the MAGIC wide-angle experiment, submitted to Journal Of South American Earth Sciences, 1srt April 2021

Pascal, G.P., Mauffret, A., Patriat, P., 1993. The ocean–continent boundary in the Gulf of Lion from analysis of expanding spread profiles and gravity modeling, Geophysical Journal International, 113, 701–726.

Pavlis, N.K., Holmes, S.A., Kenyon, S.C. and Factor, J.K., 2012. Correction to "The Development and Evaluation of the Earth Gravitational Model 2008 (EGM2008)"; Journal of Geophysical Research: SOLID EARTH, VOL. 118, 2633, doi:10.1002/jgrb.50167

Pierce, C., Whitmarsh, R.B., Scrutton, R.A., Pontoise, B., Sage, F. and Mascle, J., 1996. Côte d'Ivoire-Ghana margin: seismic imaging of passive rifted crust adjacent to a transform continental margin. Geophysical Journal International, 125: 781-795.

Rollet, N., Déverchère, J., Beslier, M.-O., Guennoc P., Réhault J.-P., Sosson M. & Truffert C., 2002. Back arc extension, tectonic inheritance and volcanism in the Ligurian Sea, western Mediterranean. Tectonics, 21, doi: 10.1029/2001TC90002

Sage, F., 1994. Structure crustale d'une marge transformante et du doaine océanique adjacent: exemple de la marge de côte d'Ivoire-Ghana. l'Universite Pierre et Marie Curie.

Sage, F., Pontoise, B., Mascle, J., Basile, C., Arnould, L., 1997. Crustal structure and ocean- continent transition at marginal ridge: the Côte d'Ivoire–Ghana marginal ridge. Geo-Mar. Lett. 17, 40–48.

Sahabi M., Aslanian D., Olivet, J.-L., Un nouveau point de départ pour l'histoire de l'Atlantique Central, C. R. A. S., 2004

Sandwell, D.T. and Smith, W.H.F., 2009. Global marine gravity from retracked Geosat and ERS-1 altimetry: Ridge segmentation versus spreading rate. Journal of Geophysical Research, 114, B01411, doi:10.1029/2008JB006008.

Séranne, M., Benedicto, A., Truffert, C., Pascal, G. & Labaume, P., 1995. Structural style and evolution of the Gulf of lion Oligo-Miocene rifting, Role of the Pyrenean orogeny. Marine and Petroleum Geology, 12, 809–820.

Séranne, M., 1999. The gulf of Lion continental margin (NW Mediterranean) revisited by IBS: an overview. In Durand, B., Jolivet, L., Horvath, F & Séranne M., (Eds), The Mediterranean Basins: Tertiary Extension Within the Alpine Orogen. Geol. Soc. of London, Special Publication, 156, 15-36.

Sibuet, J.-C. & Tucholke, B., 2012. The Geodynamic Province of Transitional Lithosphere Adjacent to Magma-Poor Continental Margins. In: Mohriak, W.U., Danforth, A., Post, P.J., Brown, D.E., Tari, G.C., Nemcok, M. & Sinha, S.T. (eds). Conjugate Divergent Margins. Geological Society, London, Special Publications, 369, doi 10.1144/SP369.15.

Tavares A.C., de Castro D. L., Bezerra F. H.R., Oliveira D.C., VannucchiP., Iacopini D., Jovane L., Vital H., 2020. The Romanche fracture zone influences the segmentation of the equatorial margin of Brazil, Journal of South American Earth Sciences,volume 103,https://doi.org/10.1016/j.jsames.2020.102738.

The International Gravimetric Bureau. In: IAG Geodesist's Handbook, -.J.o.G., V 86, N 10, Oct. 2012, Springer.

T. Tiira, U. Luosto, K. Komminaho, R. Giese, A. Guterch, C.-E. Lund, O.M. Kharitonov, T. Ilchenko, D.V. Lysynchuk, V.M. Skobelev, J.J. Doody,

Thybo, H., Janik, T., Omelchenko, V. D., Grad, M., Garetsky, R. G., Belinsky, A. A., Karatayev G.I.,Zlotski G., KnudsenM.E., Sand R. , Yliniemi J., Tiira T., Luosto U., Komminaho K., Giese R., Guterch A., Lund C.-E., Kharitonov O.M., Ilchenko T.,. Lysynchuk D.V,. Skobelev V.M, Doody, J. J., 2003. Upper lithospheric seismic ve- locity structure across the Pripyat Trough and the Ukrainian Shield along the EUROBRIDGE'97 profile. Tectonophysics, 371(1–4), 41–79. https://doi.org/10.1016/s0040-

1951(03)00200-2
Thybo, H., Artemieva, I.M., 2013. Moho and magmatic underplating in continental lithosphere. Tectonophysics, 609, 605-619.
Van Avendonk, H.J.A., Holbrook, W.S., Nunes, G.T., Shillington, D.J., Tucholke, B.E., Louden, K.E., et al., 2006. Seismic velocity structure of the rifted margin of the eastern Grand banks of Newfoundland, Canada. J. Geophys. Res. B: Solid Earth 111, 11.
Watts, A. B., Rodger, M., Peirce, C., Greenroyd, C.J. & Hobbs, R.W., 2009. Seismic structure, gravity anomalies, and flexure of the Amazon continental margin, NE Brazil. Journal of Geophysical Research, v. 114, B07103, doi:10.1029/2008JB006259.
White, R.S., McKenzie, D., O'Nions, R.K., 1992. Oceanic crustal thickness from seismic measurements and rare earth element inversions. J. Geophys. Res., 97(B13), 19683–19715.
Zelt, C.A. and Ellis, R.M., 1988. Practical and efficient ray tracing in two-dimensional media for rapid traveltime and amplitude forward modelling. Canadian Journal of Exploration Geophysics, 24: 16-31.
Zelt, C.A. and Smith, R.B., 1992. Seismic Traveltime Inversion for 2-D Crustal Velocity Structure. Geophysical Journal International, 108(1): 16-34.
Zelt C.A. and Forsyth, D.A., (1994). Modeling wide-angle seismic data for crustal structure: southeastern Grenville province, J. Geophys. Res., 99, 11 687- 11 704.
Zelt, C.A., 1999. Modelling strategies and model assesment for wide-angle seismic traveltime data. Geophysical Journal International(139): 183-204.

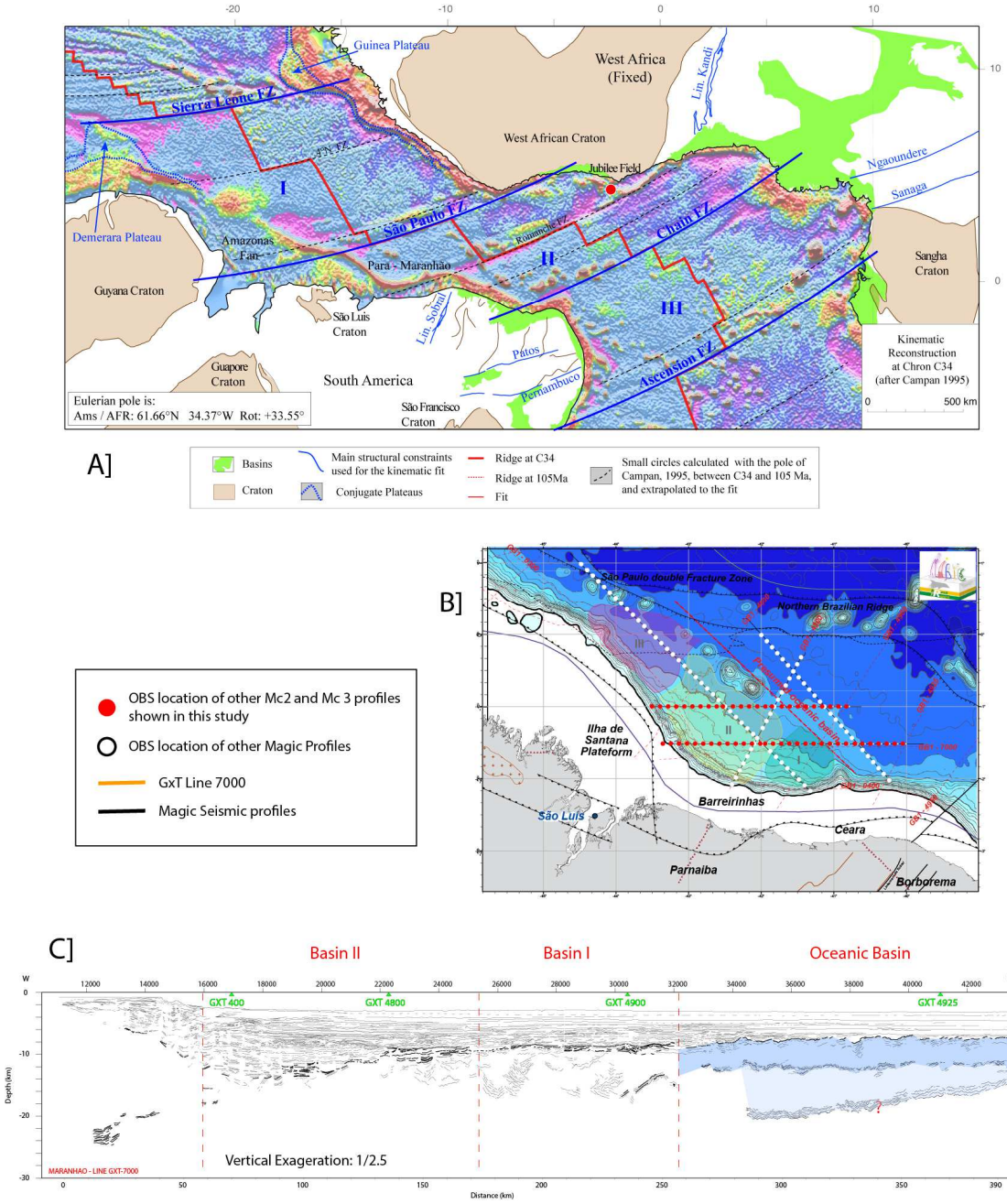

Figure 1: A) Kinematic reconstruction at C34 (Campanian), with present-day gravity data after Moulin et al. (2010), showing the segmentation of the Equatorial Segment. B) Bathymetry map of the Pará-Maranhão/Barreirinhas margin. White circles represent the OBSs deployed during the MAGIC experiment. Red Circles show the location of the OBSs presented in this study. GXT lines are indicated in red lines and labels. C) Line drawing of the depth-converted profile ION-GXT 7000, coincident with the MC3 profile.

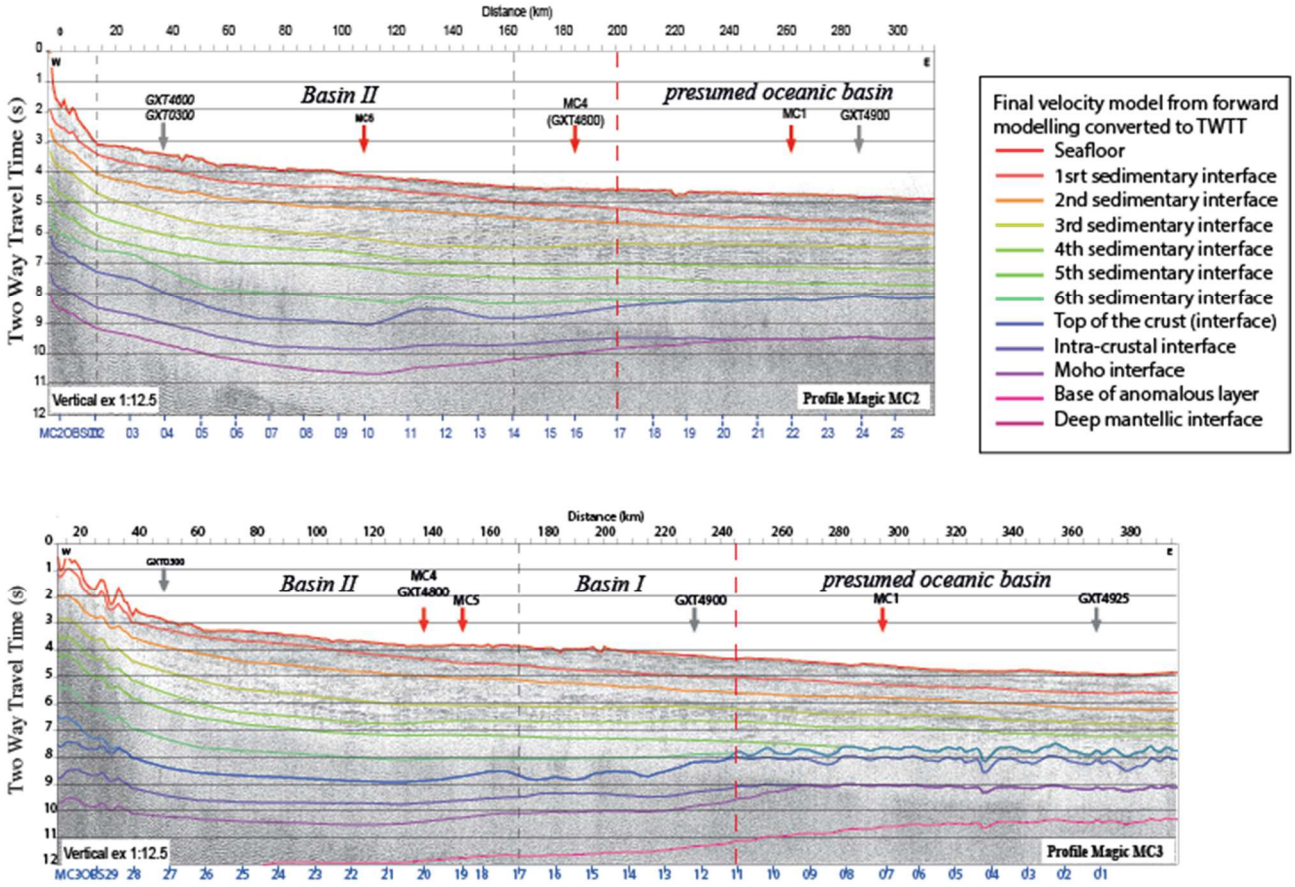

Figure 2: Multichannel seismic section of MC2 (top) and MC3 (bottom) profiles. The intersection with the Magic dataset is in red. OBSs locations are indicated in blue at the base of the profiles. The interfaces of final velocity models from forward modelling converted to TWTT is overlain. Vertical exaggeration at seafloor 1:12.5

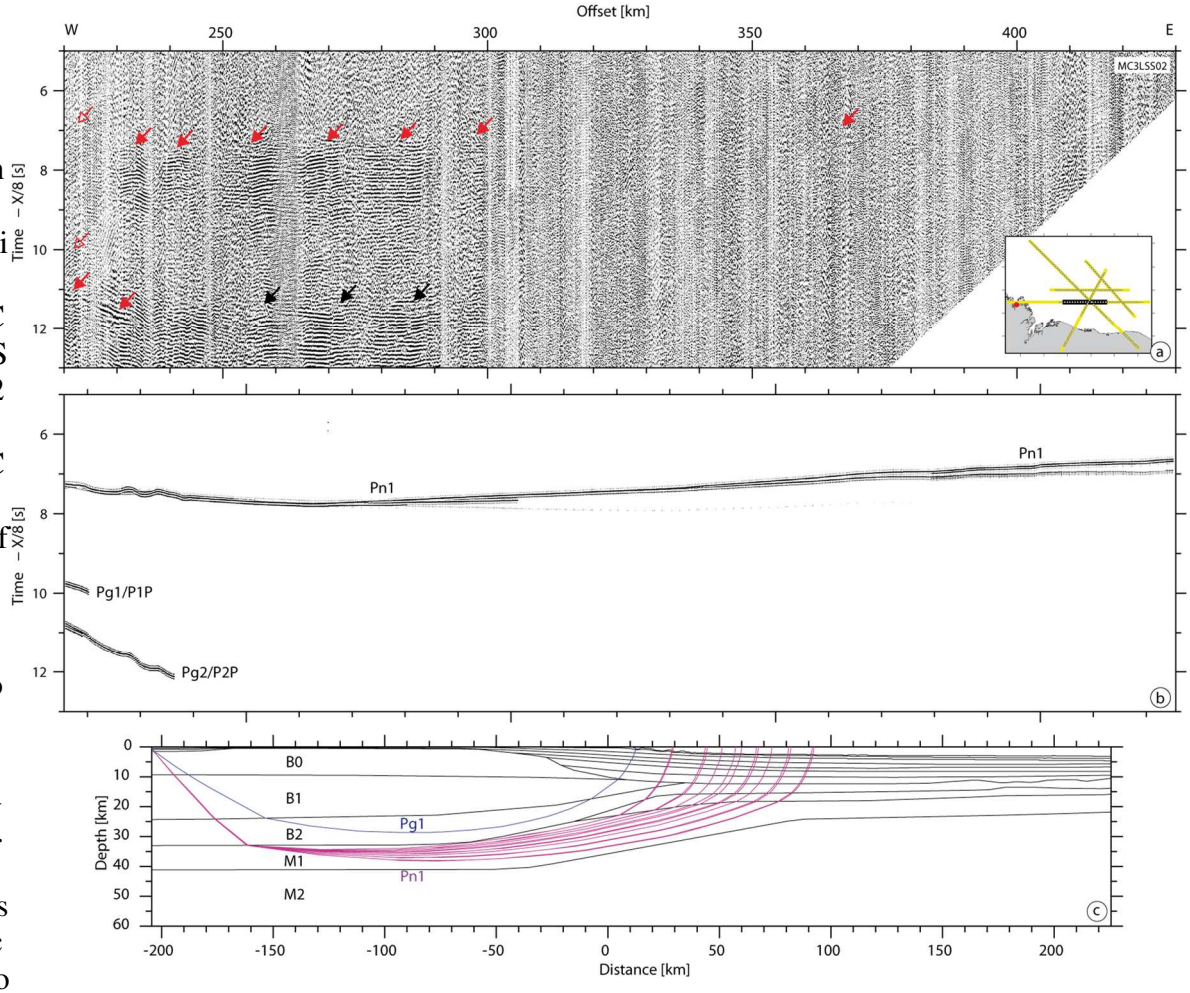

Figure 3: Land-station MC3LSS02 on MC3 profile on the São Luis Craton. a) Seismic record. The red arrows indicate the arrivals that have been used to constrain the model. The black arrows outline the second well-registered train of arrivals that might correspond to the internal multiples/reverberation of the signal. Inset map shows the positions (red dot) of the MC3LSS02; b) Synthetics; c) Seismic rays.

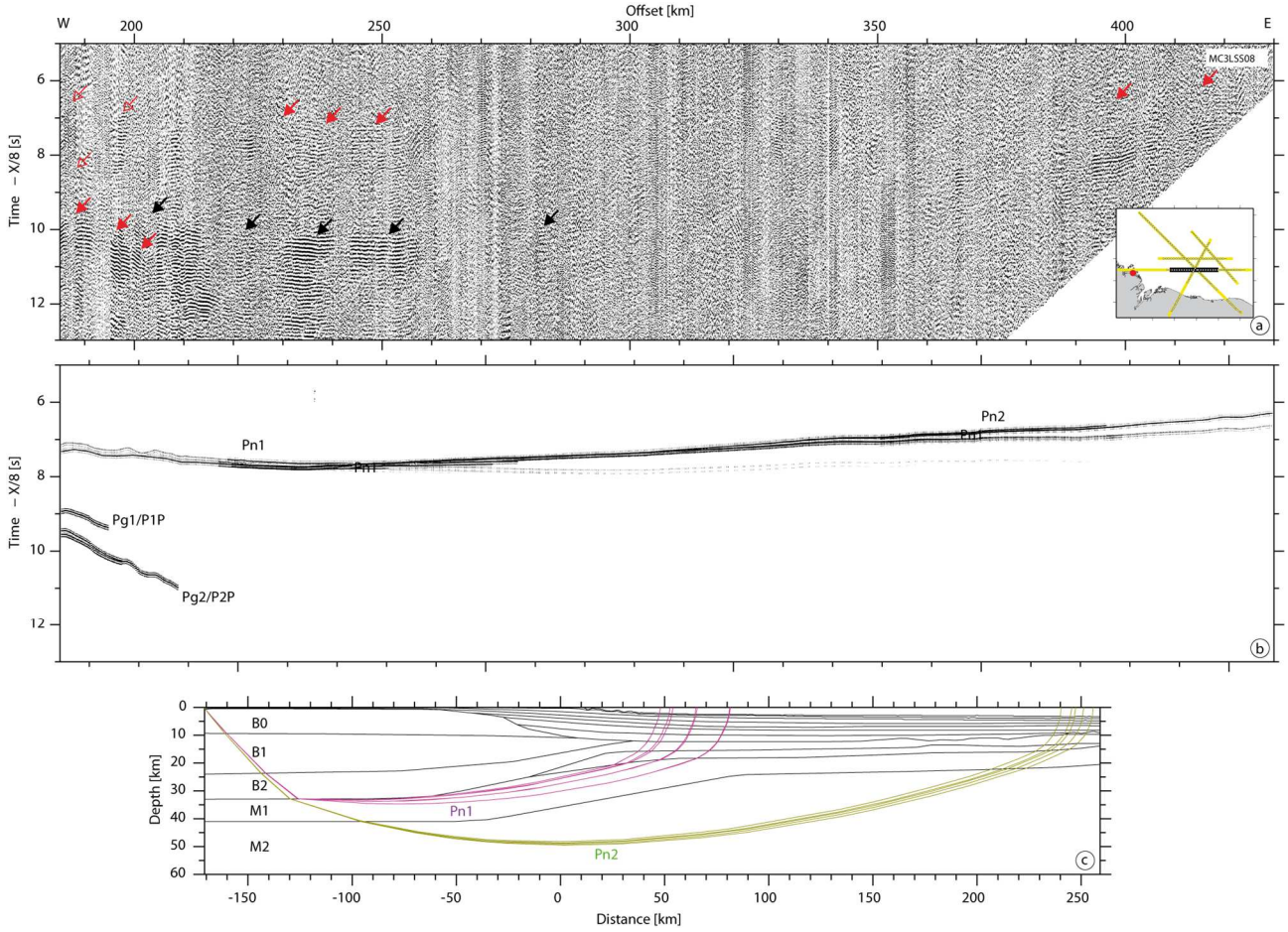

Figure 4: Land-station MC3LSS08 on MC3 profile on the São Luis Craton. a) Seismic record. The red arrows indicate the useful arrivals that have been used to constrain the model. The black arrows outline the second well-registered train of arrivals that might correspond to the internal multiples/reverberation of the signal. Inset map shows the positions (red dot) of the MC3LSS02; b) Synthetics; c) Seismic rays.

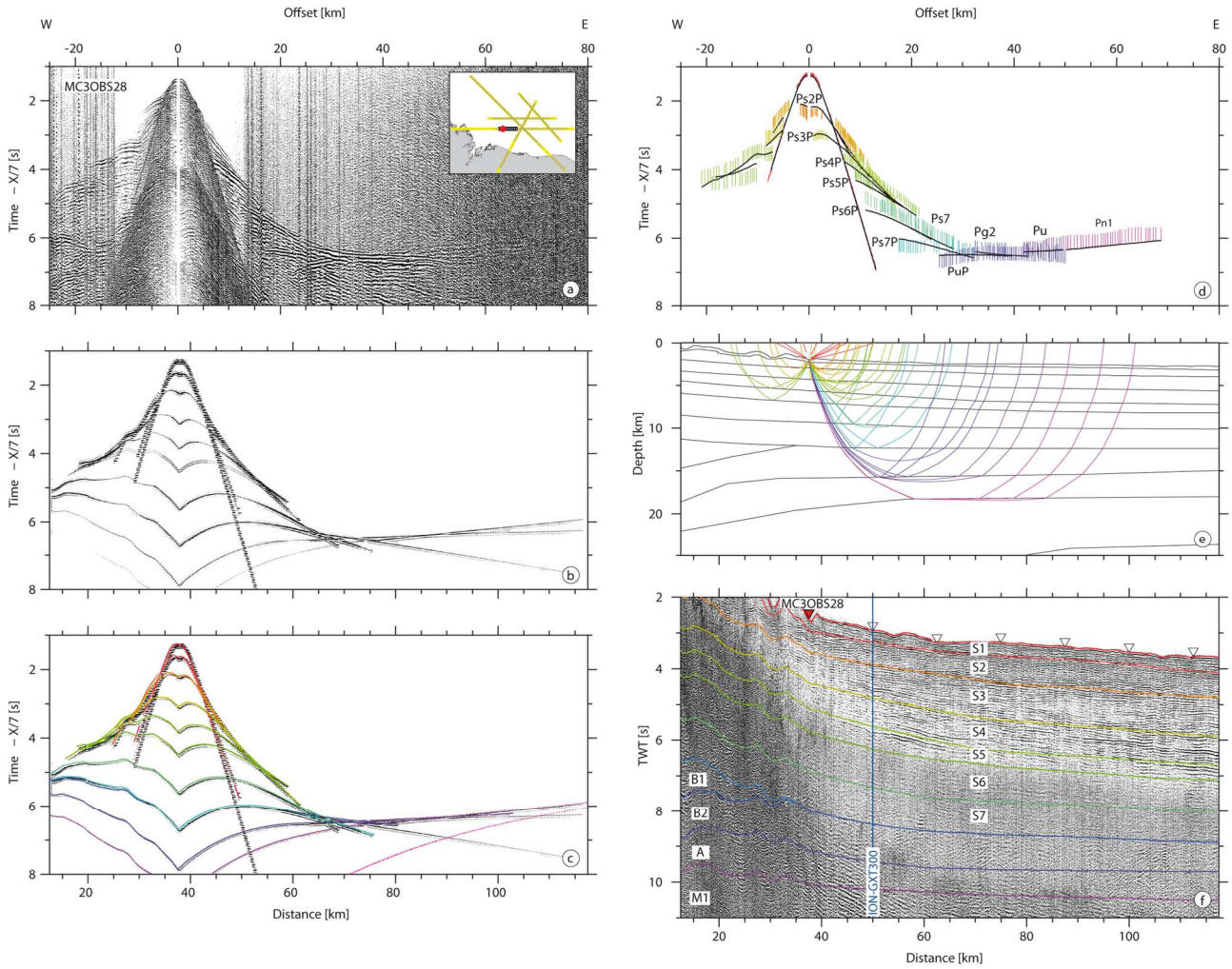

Color code and nomenclature of refracted and reflected phases

- Direct/water wave Pw
- Refraction in sedimentary layer S1 (Ps1)
- Reflection on top S2 (Ps2P)
- Refraction in sedimentary layer S2 (Ps2)
- Reflection on top S3 (Ps3P)
- Refraction in sedimentary layer S3 (Ps3)
- Reflection on top S4 (Ps4P)
- Refraction in sedimentary layer S4 (Ps4)
- Reflection on top S5 (Ps5P)
- Refraction in sedimentary layer S5 (Ps5)
- Reflection on top S6 (Ps6P)
- Refraction in sedimentary layer S6 (Ps6)
- Reflection on top S7 (Ps7P)
- Refraction in sedimentary layer S7 (Ps7)
- Reflection on top basement (Pg1P)
- Refraction in upper crust (Pg1)
- Intra-crustal reflection (Pg2P)
- Refraction in lower crust (Pg2)
- Reflection on top anormalous body (PuP)
- Refraction in anormalous body (Pu)
- Reflection on top mantle Moho (Pm1P)
- Refraction in lithospheric mantle (Pn1)
- Intra-mantlic reflection (Pm2P)
- Refraction in lithospheric mantle (Pn2)

Velocity model interfaces

- seafloor
- 1srt sedimentary interface
- 2nd sedimentary interface
- 3rd sedimentary interface
- 4th sedimentary interface
- 5th sedimentary interface
- 6th sedimentary interface
- top of the basement
- intra-crustal interface
- Moho
- base of anamalous layer (A)
- deep mantellic interface

Figure 5: MC3OBS28 on MC3 profile. East direction to the right and west to the left. a) Seismic record. Inset map shows the positions (red dot) of the MC3OBS28; b) Synthetics; c) Colour coded synthetics; d) Colour coded observed travel-times overlain by predicted times in black lines; e) Corresponding ray tracing of black lines in Figure 5d; f) MCS time migrated section and colour-coded model interfaces. On a, b, c & d, travel time is reduced by a velocity of 7 km/s.

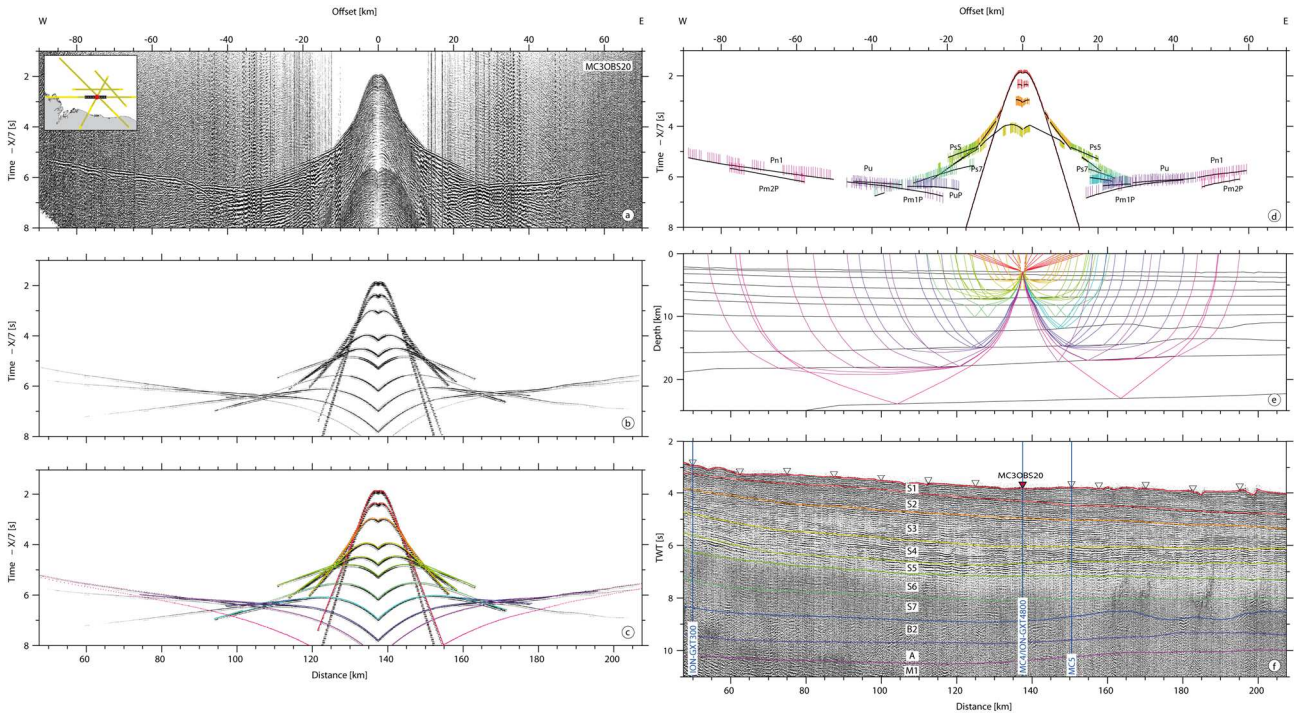

Figure 6: MC3OBS20 on MC3 profile. East direction to the right and west to the left. Same legend and colour code as Figure 5.

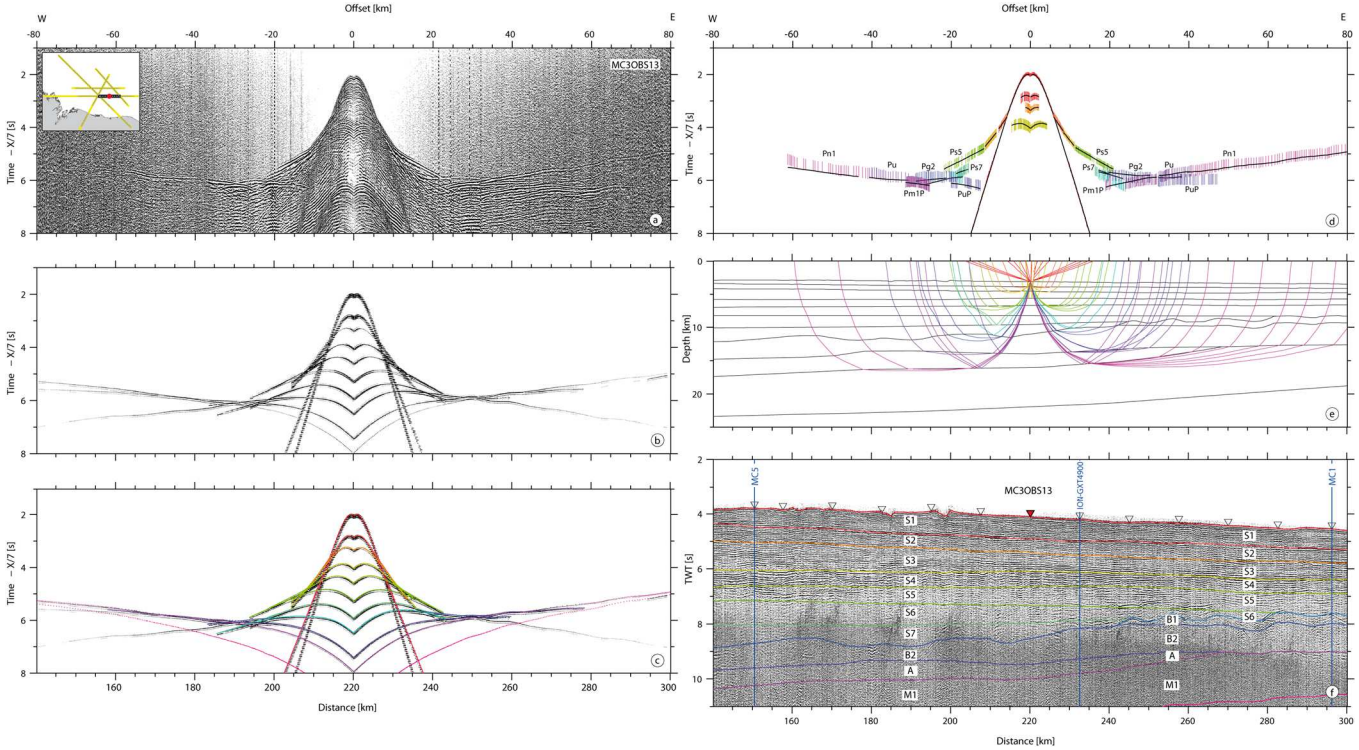

Figure 7: MC3OBS13 on MC3 profile. East direction to the right and west to the left. Same legend and colour code as Figure 5.

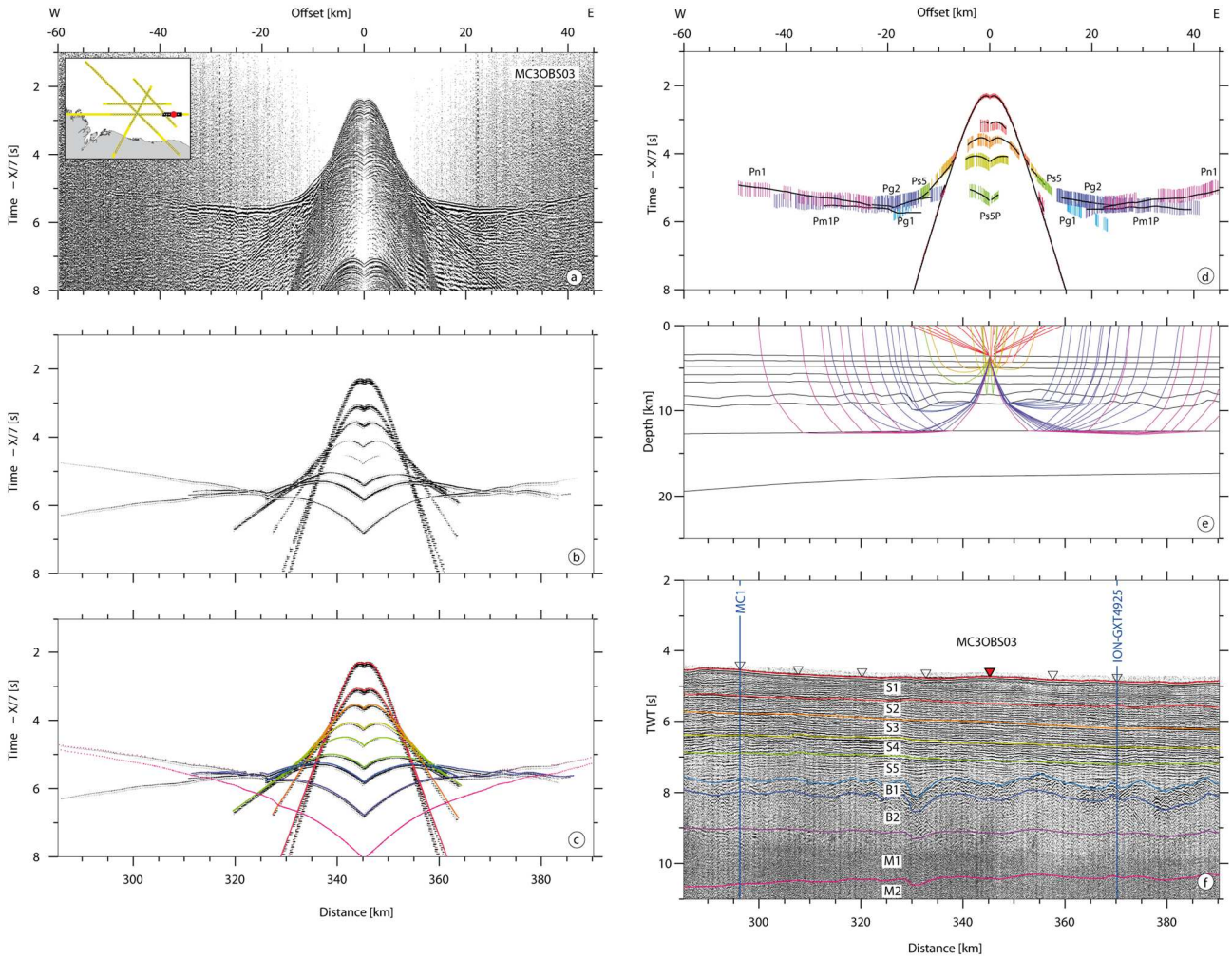

Figure 8: MC3OBSO3 on MC3 profile. East direction to the right and west to the left. Same legend and colour code as Figure 5.

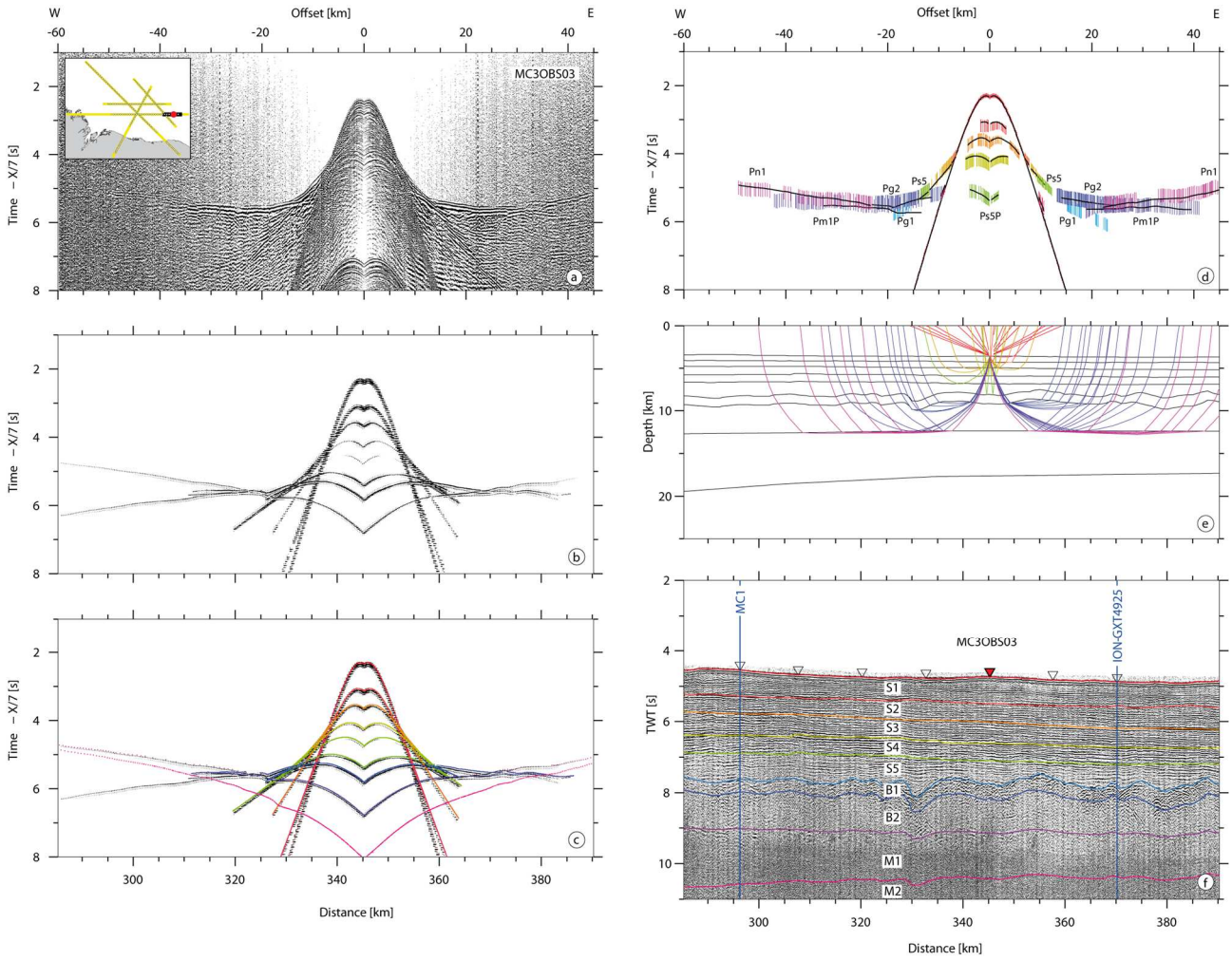
W
Offset [km]
E
-60
-40
-20
0
20
40
MC3OBS03
Time − X/7 [s]
2
4
6
8
a
b
c
Distance [km]
300
320
340
360
380
d
Pn1
Pm1P
Pg2
Pg1
Ps5
Ps5P
e
Depth [km]
0
10
20
f
TWT [s]
MC1
ION-GXT4925
S1
S2
S3
S4
S5
B1
B2
M1
M2

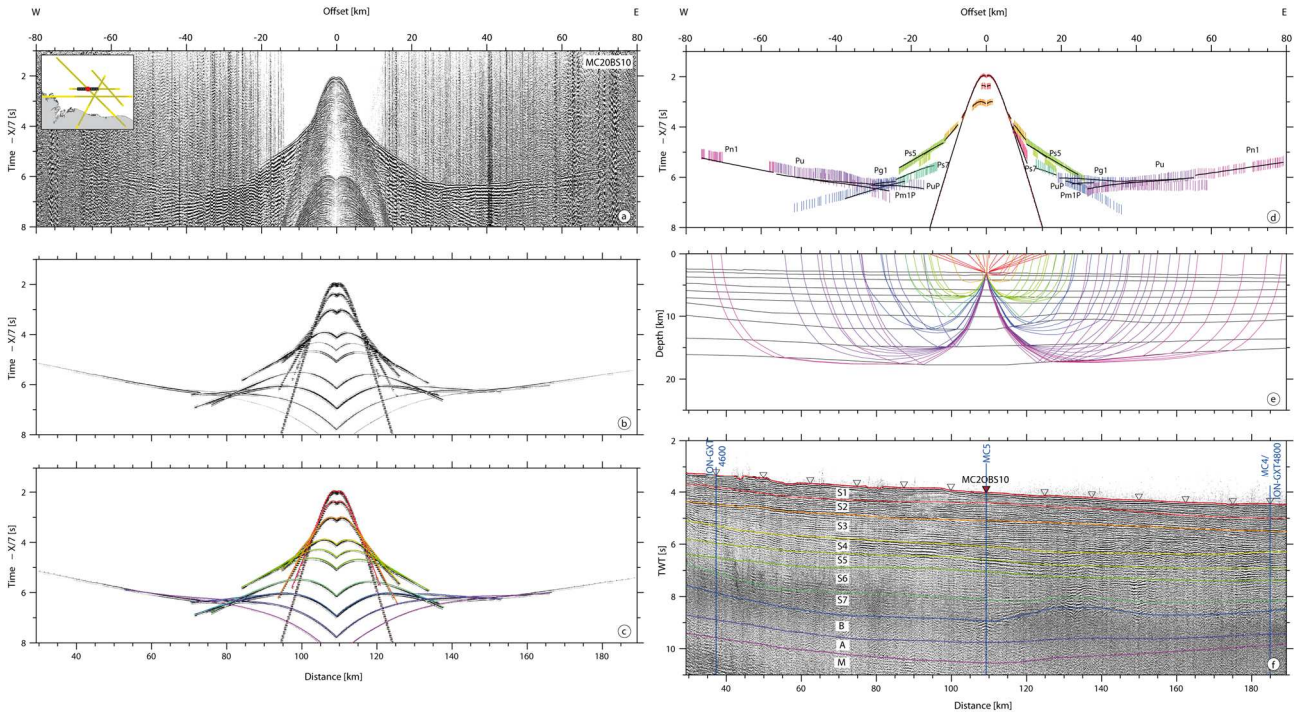

Figure 9: MC2OBS10 on MC2 profile. East direction to the right and west to the left. Same legend and colour code as Figure 5.

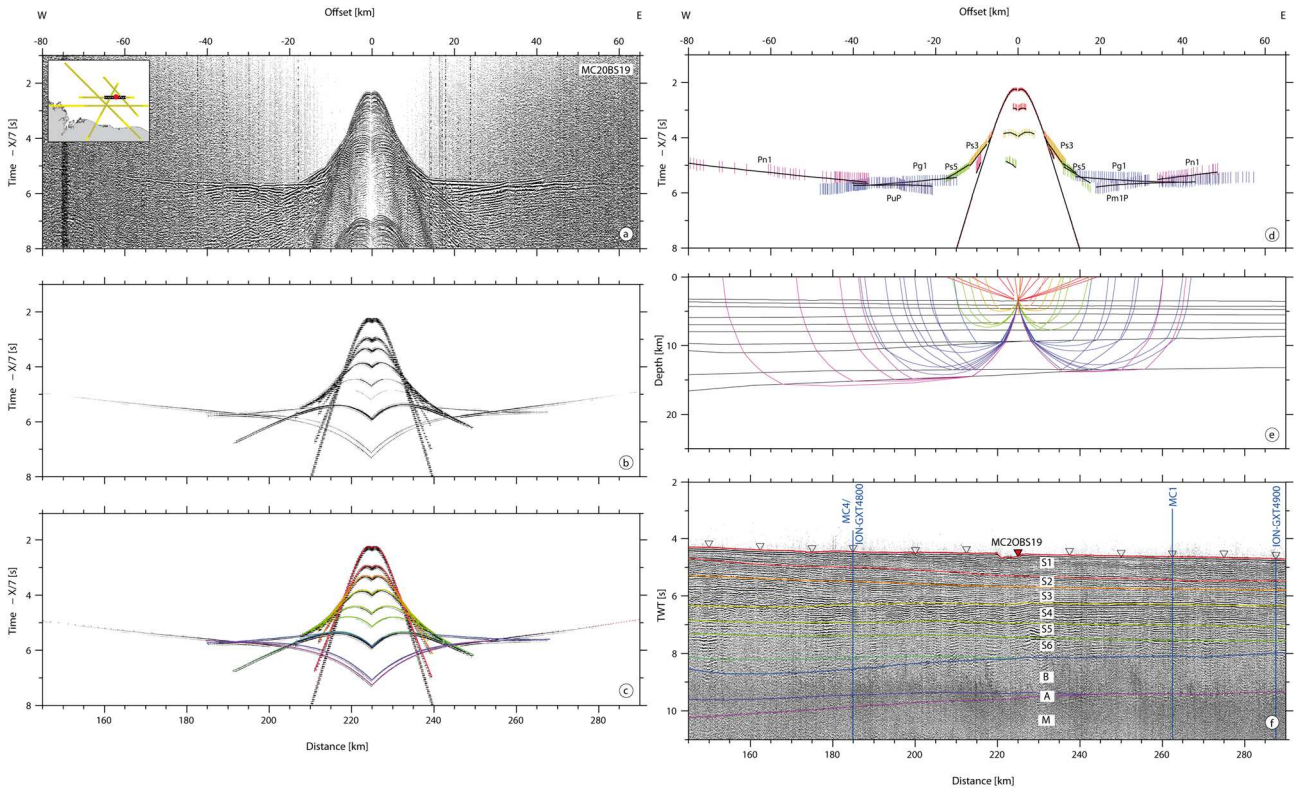

Figure 10: MC2OBS19 on MC2 profile. East direction to the right and west to the left. Same legend and colour code as Figure 5.

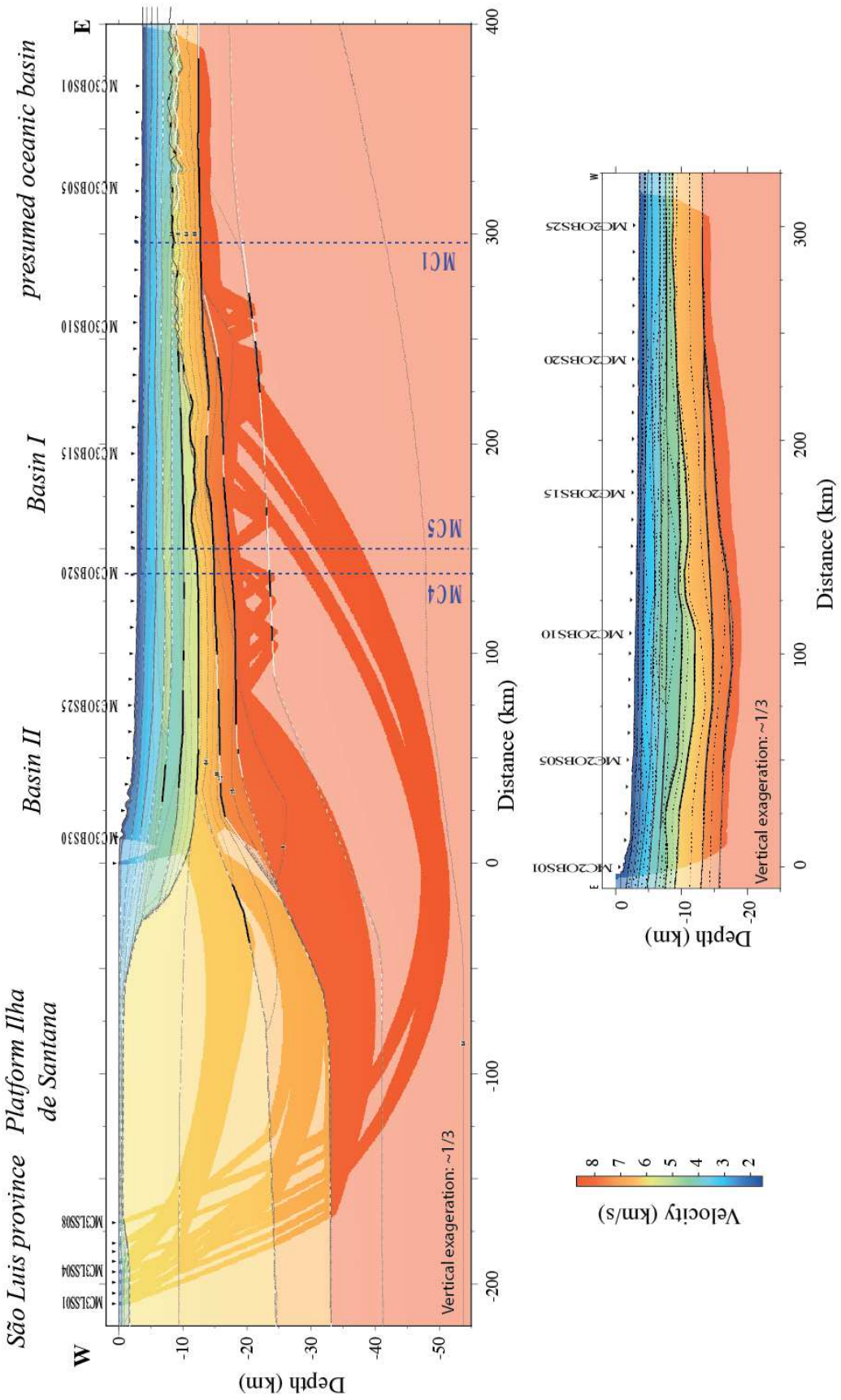

Figure 11: Final P-Wave interval velocity model along MC3 (top) and MC2 (Bottom) profiles. Black lines mark model layer boundaries. Coloured areas are constrained by seismic rays. Inverted black triangle mark OBS positions. Thin blue lines mark intersection with the other MAGIC profiles. Deep interfaces where reflections have been observed on OBS data are in thick black lines.

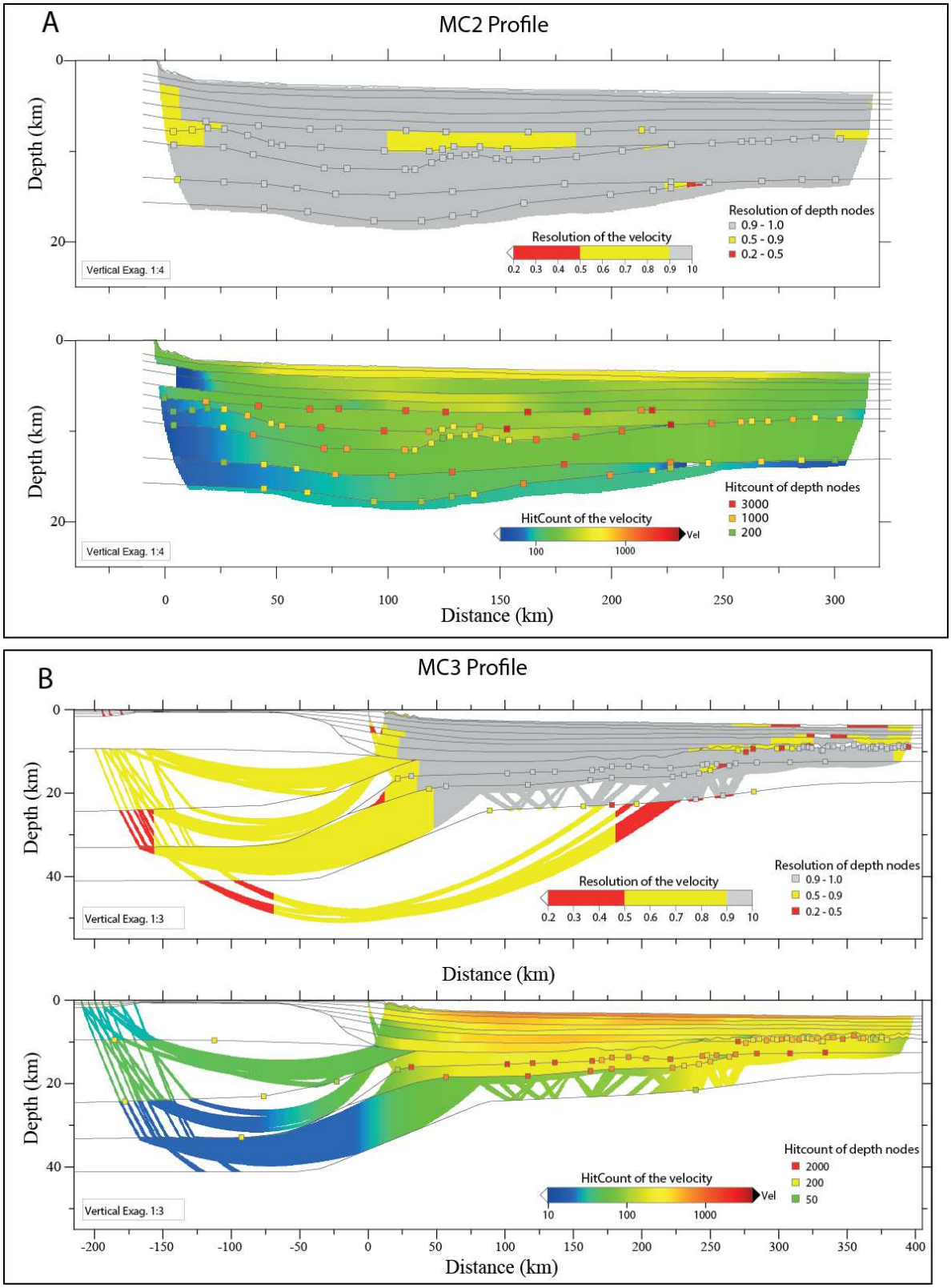

Figure 12: Evaluation of the MC2 (A) and MC3 (B) P-wave velocity models. Zones that were not imaged are blanked. For each profile are shown (Top) the Resolution of velocity (gridded and coloured) and depth nodes (coloured squares) and (Bottom) the Hit-count for velocity (gridded and coloured) and depth nodes (coloured squares). Vertical exaggeration is 1:3.

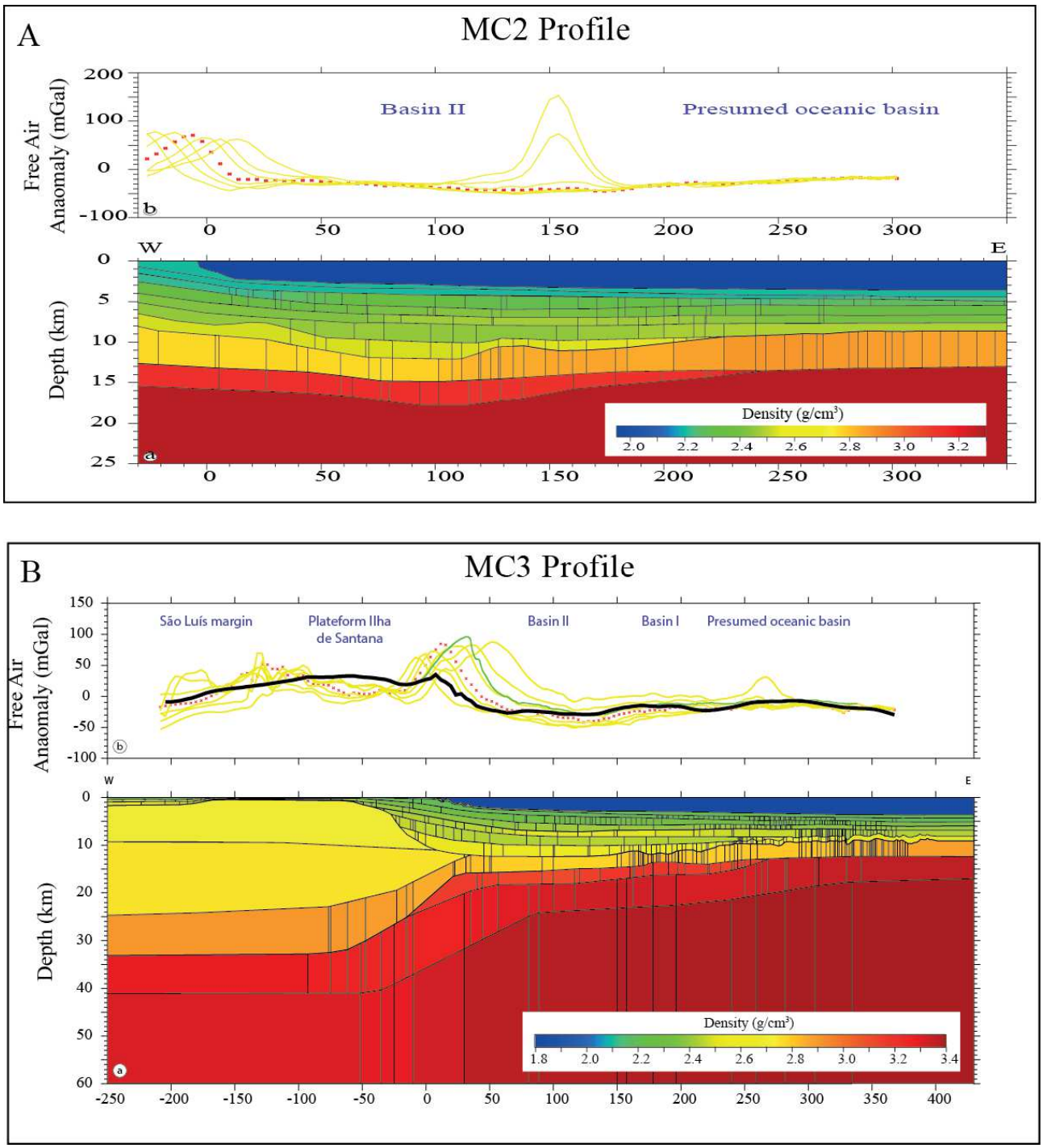

Figure 13: (A) Results of the gravity modelling of the MC2 profile with density model (bottom) respectively up to a depth of 25 km, overlain by interfaces from wide-angle modelling. Top: free-air gravity anomalies (Pavlis et al., 2012) observed along the profiles (red dotted line) and at 5, 10, 15 km on either sides (yellow lines), and calculated (black thick line).
(B) Results of the gravity modelling of the MC3 profile with density model (bottom) respectively up to a depth of 60 km, overlain by interfaces from wide-angle modelling. Top: Free-air gravity anomalies (Pavlis et al., 2012) observed along the profiles (red dotted line) and at 10, 20, 30 km on either sides (yellow lines) and calculated (black thick line). Green line: Measured gravity anomalies along the ION-GXT7000 profile.

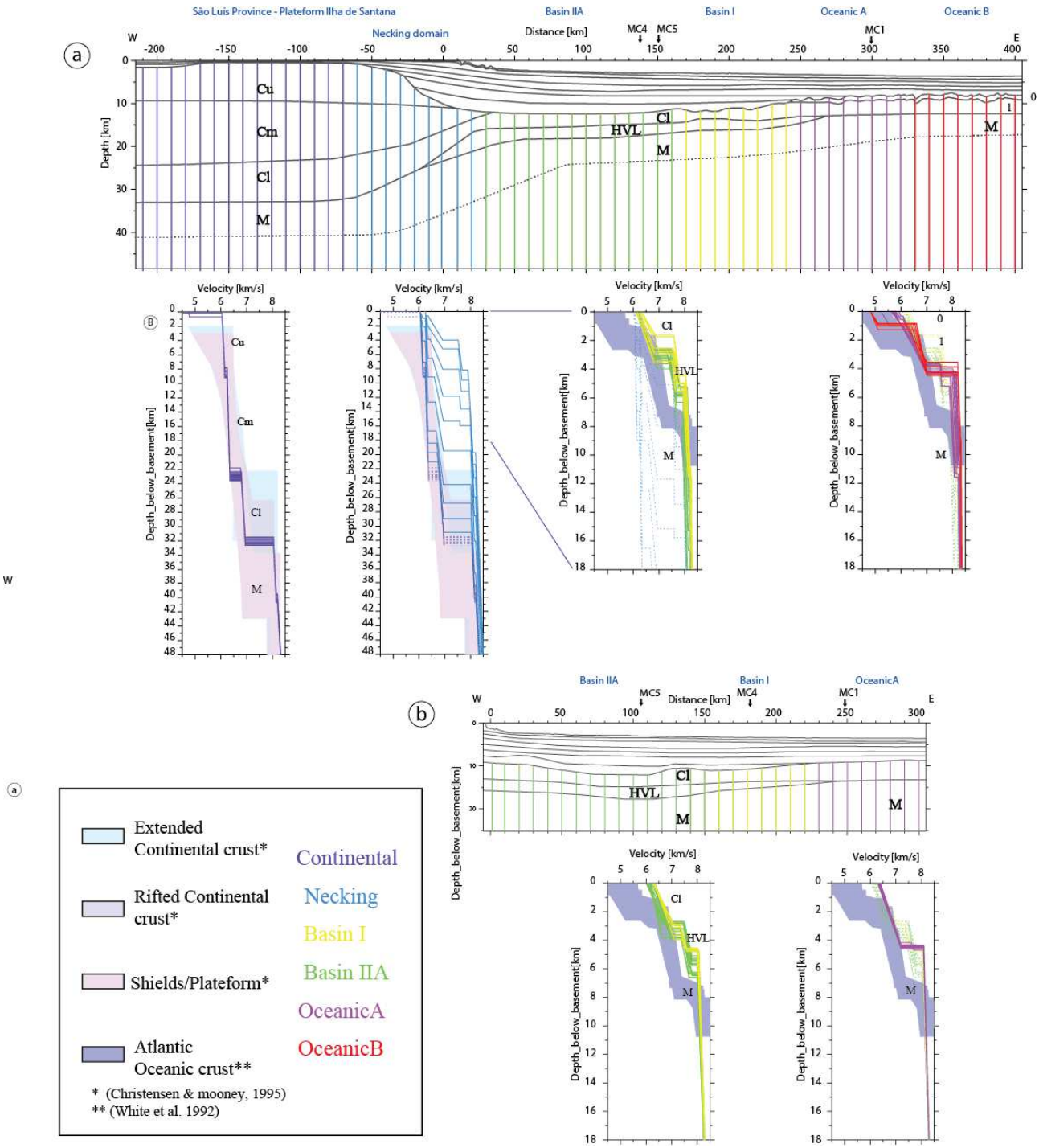

Figure 14: Distribution of 1D- velocity/depth profiles extracted every 10 km from the final P-wave velocity model showing the segmentation (colour code in legend) along MC3 (top) and MC2 (bottom) profiles. Note that the 1D- velocity/depth profiles are only extracted where the model is constrained by seismic rays.

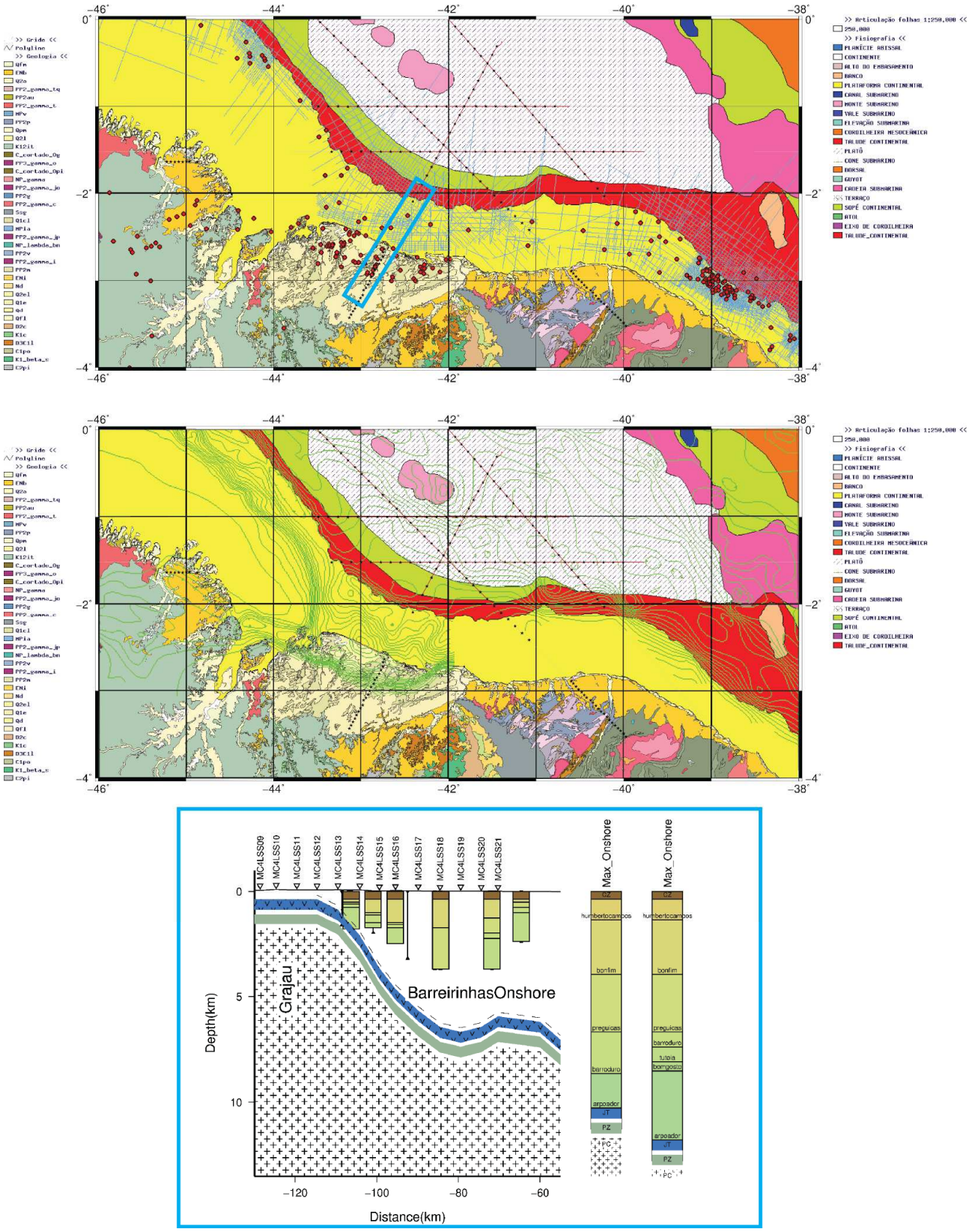

Figure 15: Top: Seismic profiles and drills location available at Geobank Brazil. Middle: Crustal depth issued from the interpretation of these data. Note the lack of data in the Ceara central domain and the middle of Ilha de Santana Platform. Bottom: Drills synthetic results of the Barreirinhas Profile from the same database (Gouyet, 1988).

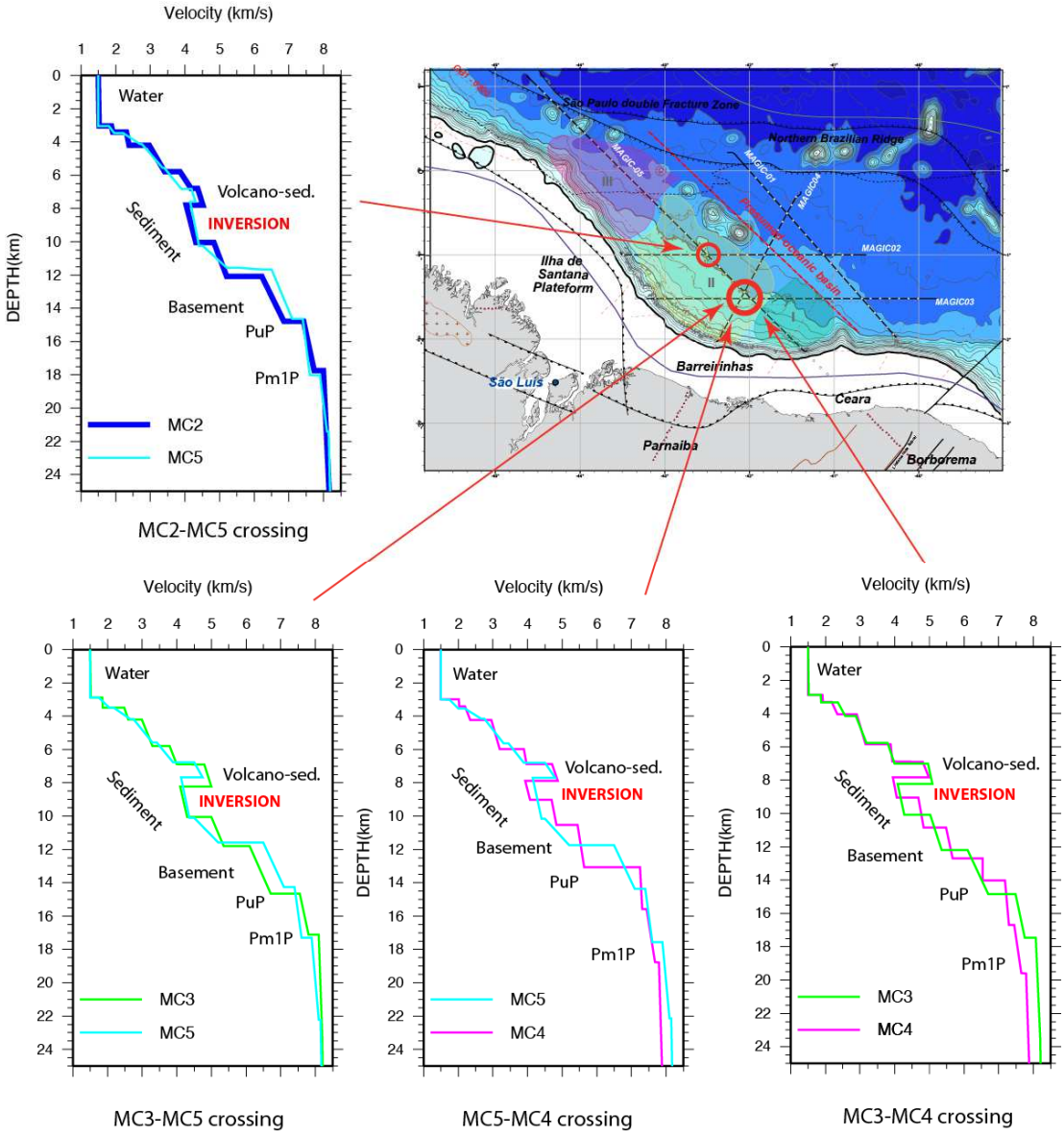

Figure 16: Total 1D-Velocity/Depth profiles (including water and sediment layers) of the four crossing points between MC2, MC3, MC4 & MC5 profiles within the deep basin.

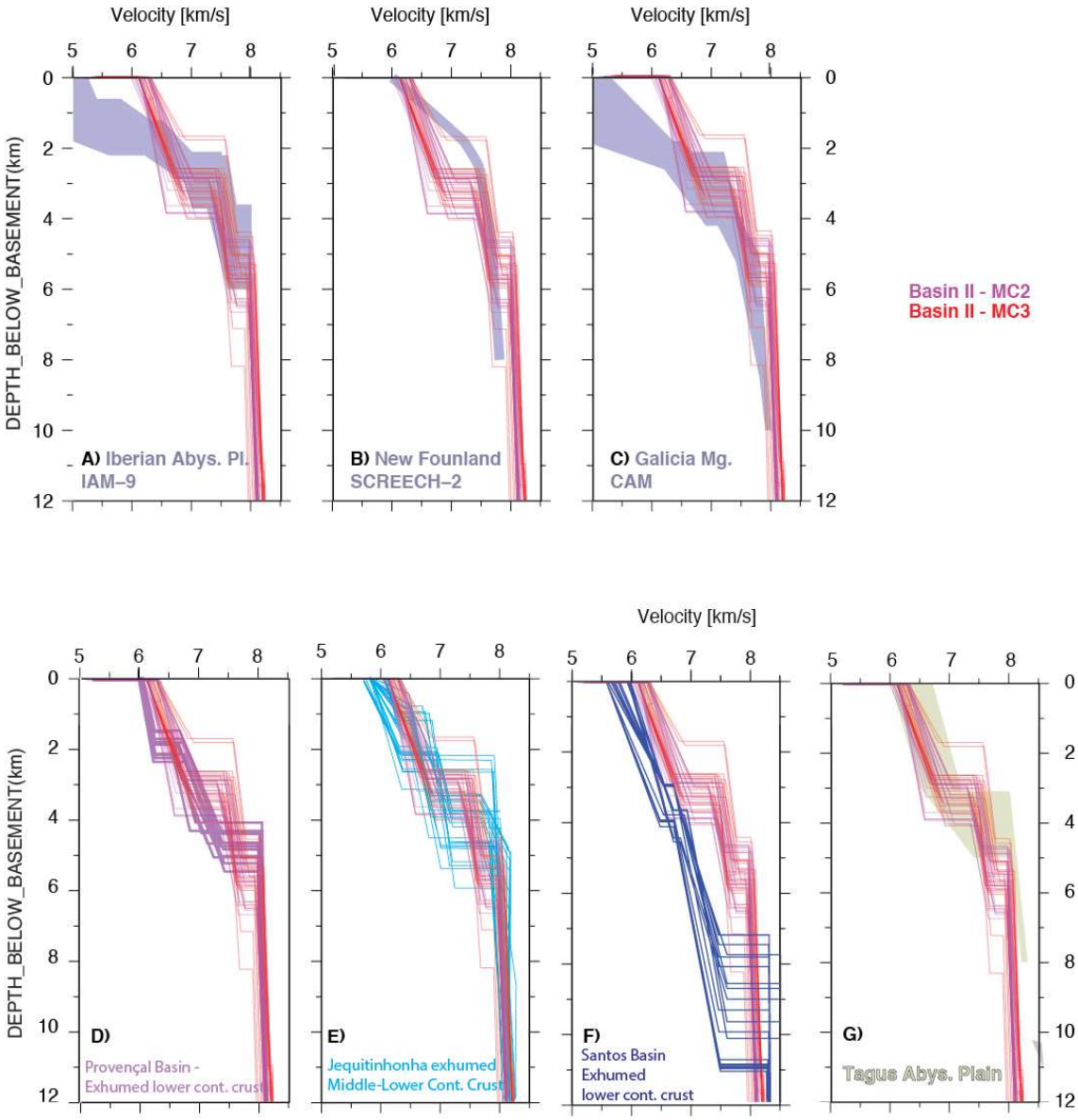

Figure 17. A-B-C — Comparison between 1D basement velocity-depth profiles of MC2 and MC3, extracted every 10 km after the necking zone and from wide-angle seismic models where ocean-transition zones were interpreted as exhumed and/or serpentinized upper mantle (shaded areas): A) in Iberia Abyssal Plain (Dean et al., 2000); B) in the Grand Banks margin, offshore Newfoundland (van Avendonk et al., 2006); C) in the Southern Galician margin (Chian et al., 1999).
D-E-F-G — Comparison between 1D basement velocity-depth profiles of MC2 and MC3, extracted every 10 km after the necking zone and from wide-angle seismic models where ocean-transition zones were interpreted exhumed middle/lower continental crust: D) in the Provençal Basin (Moulin et al., 2015; Afilhado et al, 2015); E) in the Jequitinhonha margin (Loureiro et al., 2018); F) in the Santos-Sao Paulo System (Evain et al., 2015); G) in the Tagus Abyssal Plain (Afilhado et al, 2008).

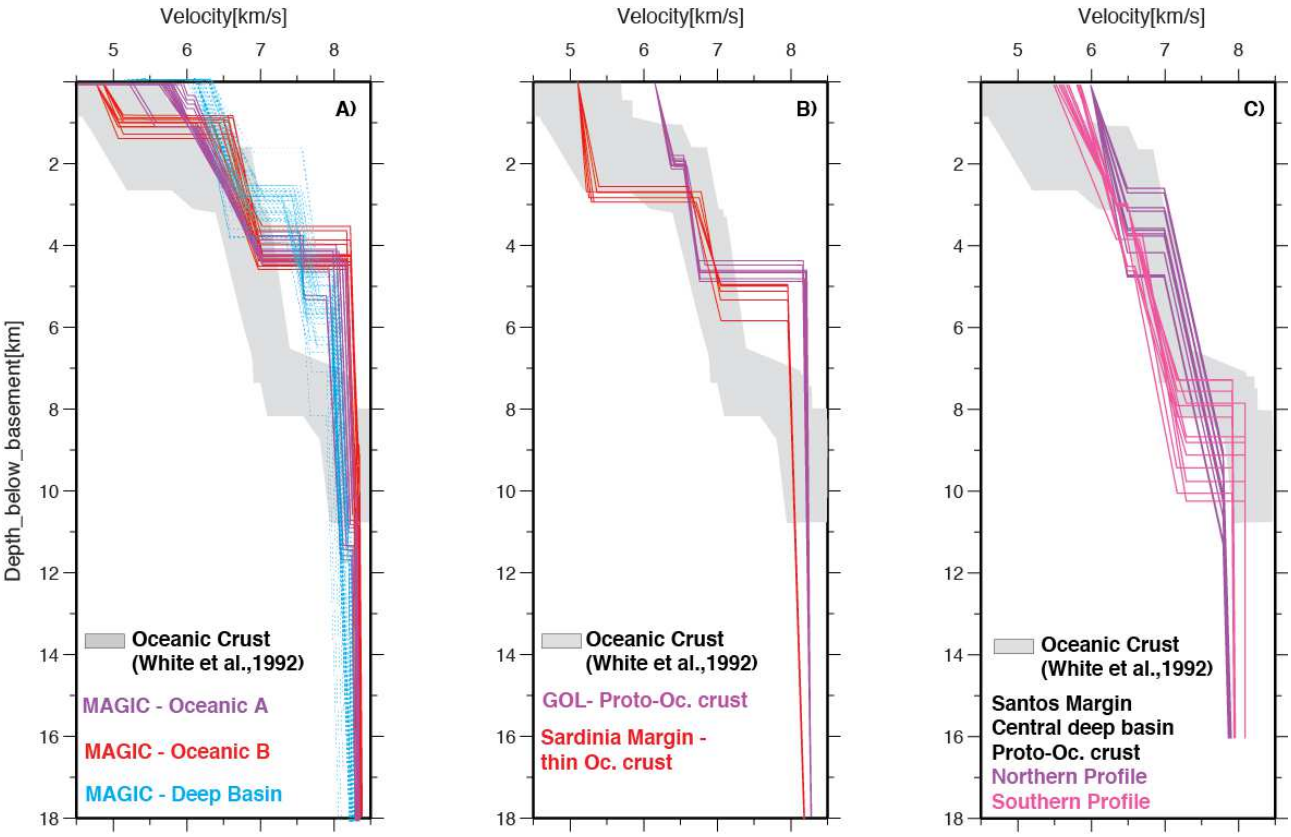

Figure 18 A- :Comparison between 1D basement velocity-depth profiles of MC2 and MC3, extracted every 10 km, in the two presumed oceanic sub-domains ; B- : Comparison between 1D basement velocity-depth profiles in the Gulf of Lion (purple lines) and the Sardinia Margin (red lines), on both sides of the Provençal Basin, in the western Mediterranean Sea (Moulin et al., 2015 ; Afilhado et al., 2015). Note the evolution from the proto-oceanic crust in the Gulf of Lion to the thin oceanic crust in the Sardinian side; C- : Comparison between 1D basement velocity-depth profiles on the northern (purple lines) and southern profiles (pink lines) in the central domain of the Santos-São Paulo system, offshore Rio de Janeiro (Evain et al., 2015). Note the evolution from the exhumed middle-lower continental crust, on the southern profile, to the proto-oceanic crust on the northern profile. These two profiles are separated by 80km.

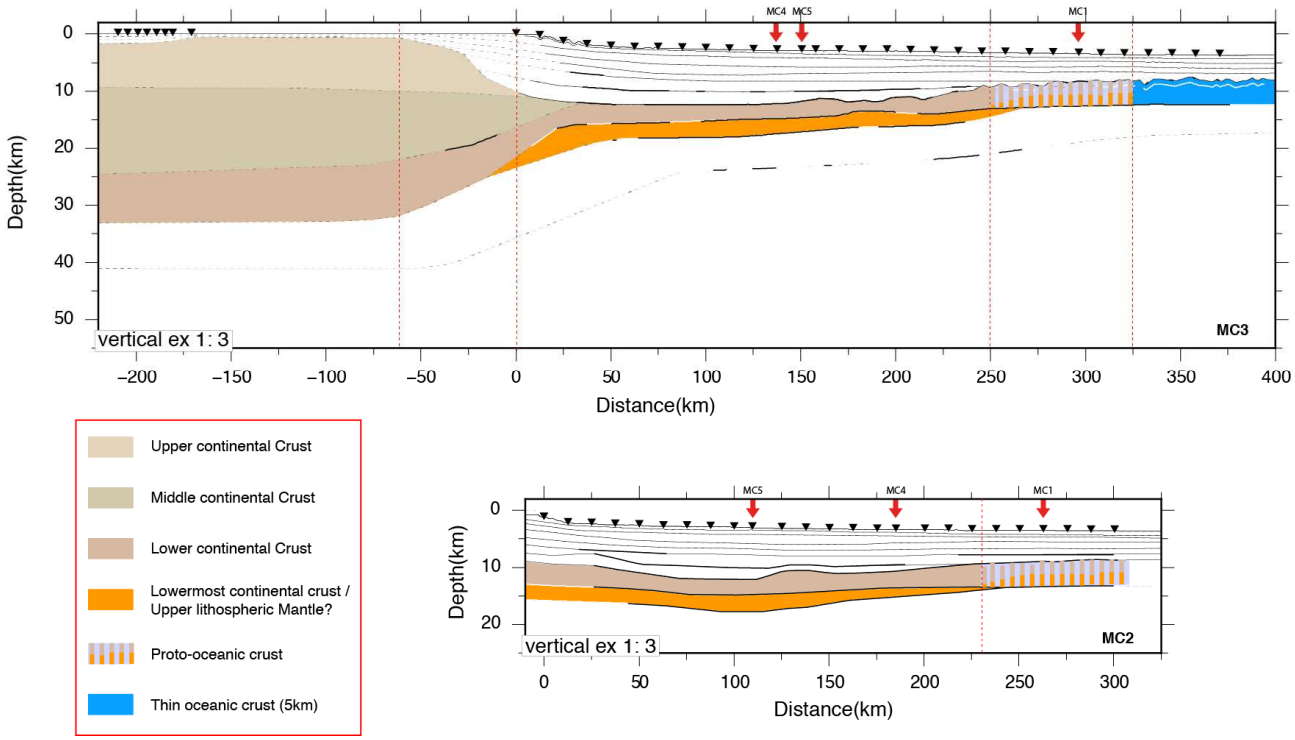

Figure 19- Geological interpretation of the MC3 (top) and MC2 (bottom) profiles. The new segmentation is shown by red dashed lines. Some interfaces appear either as thin dashed or thick dashed black lines whether their depth is resolved (resolution < 0.5) or unresolved (resolution > 0.5). Other interfaces considered as resolved are thin black lines that have been constrained by MCS data and thick black lines, which indicate where wide-angle reflections are observed. Black inverted triangles mark the OBS positions and red triangles the position of the LSS. Red arrows show the crossings between the other MAGIC profiles. Vertical exaggeration =1:3.

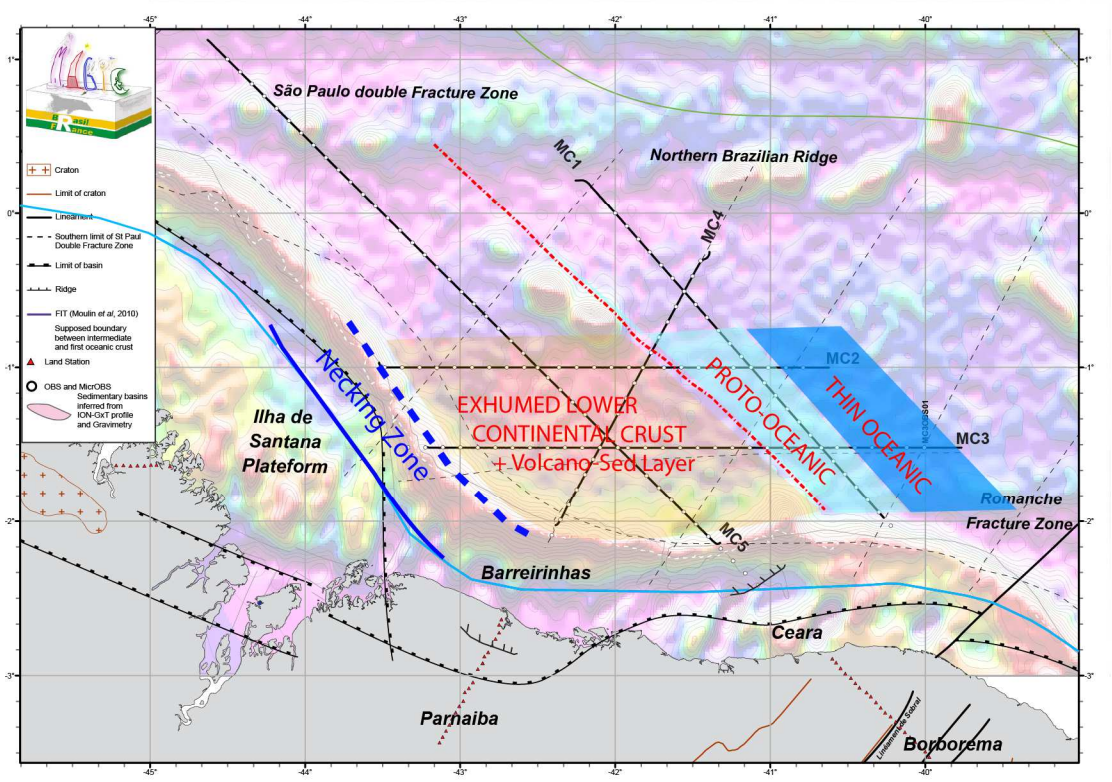

Figure 20 : Geological interpretation of the basement thanks to wide-angle data showing the E-W strong segmentation of the Pará-Maranhão/Barreirinhas passive margin. Gravity map from Sandwell & Smith (2009). The map also depicts location of MAGIC wide-angle seismic profiles (thin black lines), OBS (small white circles), Land Seismic Stations (LSS) (red triangles) and the geological crustal interpretation proposed by this study with coloured polygons (orange = exhumed lower crust; light blue = proto-oceanic crust; blue = thin oceanic crust; thick and dashed blue lines = necking zone).

		phases	number of picks	rms misfit (s)	χ^2
layer 0, water	reflected phase	Pw	3382	0.026	0.750
layer 1, sediment S1	refracted phase	Ps1	101	0.113	1.294
layer 2, sediment S2	reflected phase	Ps2P	315	0.060	1.007
	refracted phase	Ps2	322	0.073	1.465
layer 3, sediment S3	reflected phase	Ps3P	313	0.071	1.412
	refracted phase	Ps3	1024	0.139	3.142
layer 4, sediment S4	reflected phase	Ps4P	194	0.083	1.940
	refracted phase	Ps4	245	0.079	1.761
layer 5, sediment S5	reflected phase	Ps5P	119	0.066	1.238
	refracted phase	Ps5	1206	0.079	1.731
layer 6, sediment S6	refracted phase	Ps6P	328	0.091	2.296
	refracted phase	Ps6	70	0.079	0.778
layer 7, sediment S7	reflected phase	Ps7P	534	0.085	0.892
	refracted phase	Ps7	243	0.122	1.845
layer 8, crystalline basement B	reflected phase	Pg1P	517	0.090	1.006
	refracted phase	Pg1	1784	0.104	1.081
layer 9, anormalous velocity layer A	reflected phase	PuP	1121	0.086	0.740
	refracted phase	Pu	662	0.133	1.765
layer 10, upper mantle M	reflected phase	Pm1P	1055	0.134	1.805
	refracted phase	Pn1	1492	0.087	0.754

Table 1 : Number of picks, rms misfit and x2 parameters for each layer identified on MC2 model (figure 11)

		phases	number of picks	rms misfit (s)	χ^2
layer 0, water	reflected phase	Pw	5553	0.022	0.551
layer 1, sediment S1	refracted phase	Ps1	216	0.067	0.754
layer 2, sediment S2	reflected phase	Ps2P	596	0.041	0.339
	refracted phase	Ps2	582	0.047	0.618
layer 3, sediment S3	reflected phase	Ps3P	537	0.080	1.338
	refracted phase	Ps3	1607	0.083	1.572
layer 4, sediment S4	reflected phase	Ps4P	963	0.100	1.766
	refracted phase	Ps4	472	0.106	2.212
layer 5, sediment S5	reflected phase	Ps5P	496	0.107	1.693
	refracted phase	Ps5	2038	0.061	0.762
layer 6, sediment S6	refracted phase	Ps6P	139	0.149	2.826
	refracted phase	Ps6	0	X	X
layer 7, sediment S7	reflected phase	Ps7P	483	0.095	0.963
	refracted phase	Ps7	557	0.114	1.608
layer 8, crystalline basement B0	reflected phase	Pg0P	677	0.108	1.315
	refracted phase	Pg0	0	X	X
layer 9, crystalline basement B1	reflected phase	Pg1P	0	X	X
	refracted phase	Pg1	316	0.189	1.487
layer 10, crystalline basement B2	reflected phase	Pg2P	89	0.188	3.593
	refracted phase	Pg2	1677	0.081	0.569
layer 11, anormalous velocity layer A	reflected phase	PuP	1814	0.107	1.145
	refracted phase	Pu	1039	0.094	0.880
layer 12, upper mantle M1	reflected phase	Pm1P	850	0.089	0.786
	refracted phase	Pn1	2929	0.107	1.005
layer 13, mantle M2	reflected phase	Pm2P	172	0.119	1.416
	refracted phase	Pn2	23	0.211	1.161

Table 2: Number of picks, rms misfit and x2 parameters for each layer identified on MC3 model (figure 11)